Journal of Nanobiotechnology

RESEARCH Open Access

Microenvironment-optimized gastrodin-functionalized scaffolds orchestrate asymmetric division of recruited stem cells in endogenous bone regeneration

Shilin Pan[1†], Yao Li[2†], Lu Wang[1], Yingchao Guan[1], Kaiyang Xv[1], Qing Li[1], Guangli Feng[3], Yingrui Hu[1], Xiaoqian Lan[3], Shiyi Qin[3], Li Gui[4*] and Limei Li[1*]

Abstract

The regeneration of osteoporotic bone defects remains challenging as the critical stem cell function is impaired by inflammatory microenvironment. Synthetic materials that intrinsically direct osteo-differentiation versus self-renewal of recruited stem cell represent a promising alternative strategy for endogenous bone formation. Therefore, a microenvironmentally optimized polyurethane (PU) /n-HA scaffold to enable sustained delivery of gastrodin is engineered to study its effect on the osteogenic fate of stem cells. It exhibited interconnected porous networks and an elevated sequential gastrodin release pattern to match immune-osteo cascade concurrent with progressive degradation of materials. In a critical-sized femur defect model of osteoporotic rat, 5% gastrodin-PU/n-HA potently promoted neo-bone regeneration by facilitating M2 macrophage polarization and $CD146^+$ host stem cell recruitment to defective site. The implantation time-dependently increased the bone marrow mesenchymal stem cell (BMSC) population, and further culture of BMSCs showed a robust ability of proliferation, migration, and mitochondrial resurgence. Of note, some of cell pairs produced one stemness daughter cell while the other committed to osteogenic lineage in an asymmetric cell division (ACD) manner, and a much more compelling ACD response was triggered when 5% gastrodin-PU/n-HA implanted. Further investigation revealed that one-sided concentrated presentation of aPKC and β-catenin in dividing cells effectively induced asymmetric distribution, which polarized aPKC biased the response of the daughter cells to Wnt signal. The asymmetric cell division in skeletal stem cells (SSCs) was mechanically comparable to BMSCs and also governed by distinct aPKC and β-catenin biases. Concomitantly, delayed bone loss adjacent to the implant partly alleviated development of osteoporosis. In conclusion, our findings provide insight into the regulation of macrophage polarization combined

[†]Shilin Pan and Yao Li contributed equally to this work.

*Correspondence:
Li Gui
guili0527@126.com
Limei Li
scullm@163.com

Full list of author information is available at the end of the article

with osteogenic commitment of recruited stem cells in an ACD manner, advancing scaffold design strategy for endogenous bone regeneration.

Graphical abstract

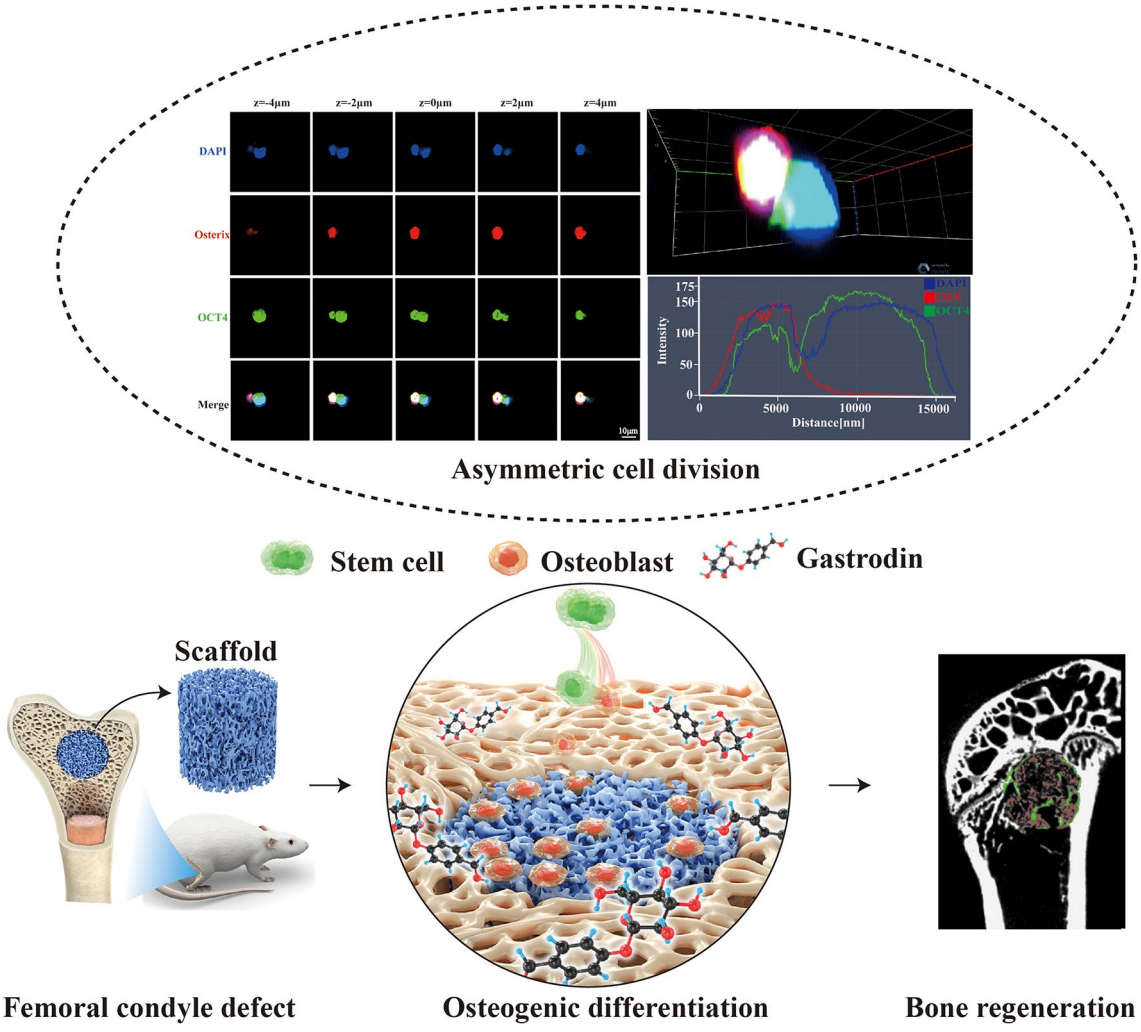

Keywords Gastrodin delivery, Microenvironment regulation, Asymmetric cell division, Osteogenic differentiation, Endogenous bone regeneration

Introduction

Treatment of large bone defects has been a challenging task because it involves cells from multiple systems. In the field of tissue engineering, biomaterials have been employed as the vehicle for stem cells or delivery of bioactive ingredients as well as the core template for cellular activities and tissue regeneration [1–3]. The reemerging structures and composition at the defect sites may provide necessary bioactive cues to create an appropriate niche for the migration, proliferation, and differentiation of stem cells. To date, tissue engineering has dominated attempts to construct functional bone scaffolds that can recruit stem/progenitor cells in situ and provide a microenvironment that induce their osteogenic differentiation for endogenous bone regeneration. This approach can circumvent problem such as in vitro inadequate expansion efficiency and the subsequent in vivo lineage commitment after exogenous stem cell transplantation.

Stem cells underpin the major functions of the bone, a majority of which adjoin blood vessels or reside in mesenchyme. In response to fracture injury at the biomaterial implantation site, the endogenous stem cells or progenitors are activated and migrate to the lesion *via* damage-associated molecular patterns, including cytokines, and chemokines [4–6]. Among them, the chemokine stromal cell-derived factor 1α (SDF-1α) was described

to recruit autologous stem cells from surrounding tissue and peripheral blood to target sites by the SDF-1α/CXCR4 pathway but failed in the long-term treatment [7]. Beyond that, the osteogenic subpopulations of stem cells that increase in number are rapidly dividing and short-lived after bone fracture, and are significantly depleted during inflammation [8]. The limited numbers of endogenous stem cells are insufficient for complete bone regeneration, especially in osteoporotic individuals [6]. It is surprising that immune response is widely recognized as the pivotal factor that has not been taken into account to determine the outcome of bone regeneration. As a crucial effector cell of innate immune system, macrophages are the early responders and tend to polarize into pro-inflammatory M1-like phenotype, a dominant player in progenitor cell recruitment within the defect site [9]. Inevitably, excessive production of pro-inflammatory mediators by M1 phenotype can lead to dysfunction and stem cell apoptosis thereby increasing the risk of delayed bone healing [10]. On the other hand, in a microenvironment that promotes M2 polarization, macrophages secrete cytokines such as interleukin-4 (IL-4), interleukin-10 (IL-10), transforming growth factor-β (TGF-β) and bone morphogenetic protein-2 (BMP-2) that contribute to proliferation and effective mineralization of osteoblasts [9, 11]. Therefore, it would be an effective strategy to recruit sufficient endogenous stem cells with early enrichment of M2-type macrophages to protect functional stem cells and neonatal osteoblasts from delayed apoptosis. Given the importance of macrophages in biomaterial-mediated osteo-immunomodulation, engineering macrophages-responsive biomaterial has become an alternative and, indeed, an attractive strategy.

Gastrodin, a primary bioactive constituent of traditional Chinese herbal medicine with potential anti-inflammatory/immune capacities [12, 13], has long been recognized an inherent drug for therapeutic development [14]. This has been described to involve MAPK, Notch and Wnt/β-catenin signaling pathways [15–17]. We have previously reported several regulatory and stimulatory effects of gastrodin-release system on M2-type macrophages. Polyurethane-nano hydroxyapatite (PU/n-HA) complexes in this context allow localized activity of gastrodin within a composite that is permissive for cellular orchestration, producing an ameliorative and pro-healing microenvironment for bone regeneration [18]. Composite scaffolds, a 3D template, are able to promote new tissue growth through provision of environmental cues that direct stem cell function. Therefore, the construction of functional porous scaffolds capable of releasing gastrodin sequentially to induce endogenous bone regeneration represent a crucial facet of in situ tissue engineering. Despite its increasing prevalence in tissue engineering, the cooperative functions of drug release and progressive degradation are unmatched; hence, it is hard to satisfy the endogenous cascades of bone regeneration. Therefore, a microenvironmentally optimized gastrodin-functionalized scaffold is desirable. Adding to this conundrum is the fact that the precise mechanism guiding the stem cell fate has remained poorly defined.

Asymmetric cell division (ACD) of stem cell has emerged as an important means of balancing self-renewal and differentiation in bone fracture healing, with the production of one stem cell and one differentiating cell to maintain tissue homeostasis. When the stem cells are affected by an injury, the asymmetric environmental signals are established and the polar regulatory proteins (par3/par6/aPKC, Fizzled/Dishevelled/Diego complex, etc.) form local aggregation to ensure binary outcomes of the fate determination [19]. They further enrich other proteins for function, and produce precursors and differentiated daughter cells to meet the needs of microenvironment repair, while the other daughters retreat back into quiescence, thus preserving the stem cell population [20]. As demonstrated in different types of mammalian stem cells, such as satellite cells and neuroblast stem cell, par complex mediated ACD ensures cellular diversity and tissue homeostasis throughout evolution [21, 22]. Wnt is characterized as the main regulator in bone biology and disease. It is governed by a protein family of secreted growth factors, favorable for proliferative stem and progenitor cells to repair tissue [23, 24]. Recent studies have shown that the local delivery of Wnt3a soaked in hydrogel carriers [25] or covalently bound onto platforms [26] had capability of balancing stemness maintenance and osteogenic differentiation by ACD induction. The promotive ACD effect was also triggered by the well-known strontium treatment [27], pointing at the crucial role of ACD process in tissue engineering.

Thus, the recruitment of stem cells to defect areas by osteo-immunoregulation and induction of osteogenic differentiation by asymmetric division are essential to boost the endogenous bone regeneration. It was hypothesized that gastrodin-PU/n-HA scaffold might regulate the polarization of macrophages into M2 phenotype and form an osteogenic microenvironment, thereby promoting osteogenesis in the osteoporotic bone defects. Meanwhile, its anti-oxidative stress function may enhance the self-renewal ability and transcriptomic diversity of stem cells, which is often diminished in adult bone tissues or even exhausted in aged individuals. In light of the above, this study was aimed to develop a strategy to determine whether gastrodin-PU/n-HA that would direct stem cells to the injured sites as well as accurately match the mechanism of bone regeneration process. We focused on how the scaffold might precisely balance the stem cell population and differentiation directed by ACD process. The system may recruit and empower endogenous

stem/progenitor cells, while maintaining stem cell pool, and expanding large numbers of specific subpopulations with osteogenic potential for more efficient tissue repair. It is envisaged that the biomaterial-mediated ACD strategy presented in this study will bring new inspiration for the development of bone-regenerative biomaterials (See Scheme 1).

Materials and methods

Study design

As the most commonly used biological evaluation method, both the bone regeneration effects in vivo and cellular experiments in vitro play an important role in the functional study of biomaterials. However, little is known of the fate and bioactivity of cell response to the implant. It is imperative to decipher the distinct fate of stem cells after scaffold therapy during the regeneration of defective bone. This study was aimed to develop a strategy to identify endogenous bone regeneration mechanism triggered by gastrodin-PU/n-HA. The scaffolds were prepared as osteoinductive implants to guide the regeneration of osteoporotic bone defects. The scaffolds were then implanted into condyles of femur in an osteoporotic rat model. The changes in serum and tissue inflammatory markers were first monitored during implantation. Furthermore, sequential cell extraction was carried out to explore the cell recruitment and reveal the time course of stem cell fate, focusing on the balance between stem cell population and osteo-differentiation *via* ACD. New bone regeneration within and adjacent to the scaffolds was finally assessed by micro-computed tomography (micro-CT) scanning and histological staining. Subsequently, histological, immunohistochemical (IHC) staining were conducted to explore the potential osteogenic mechanism of the scaffolds.

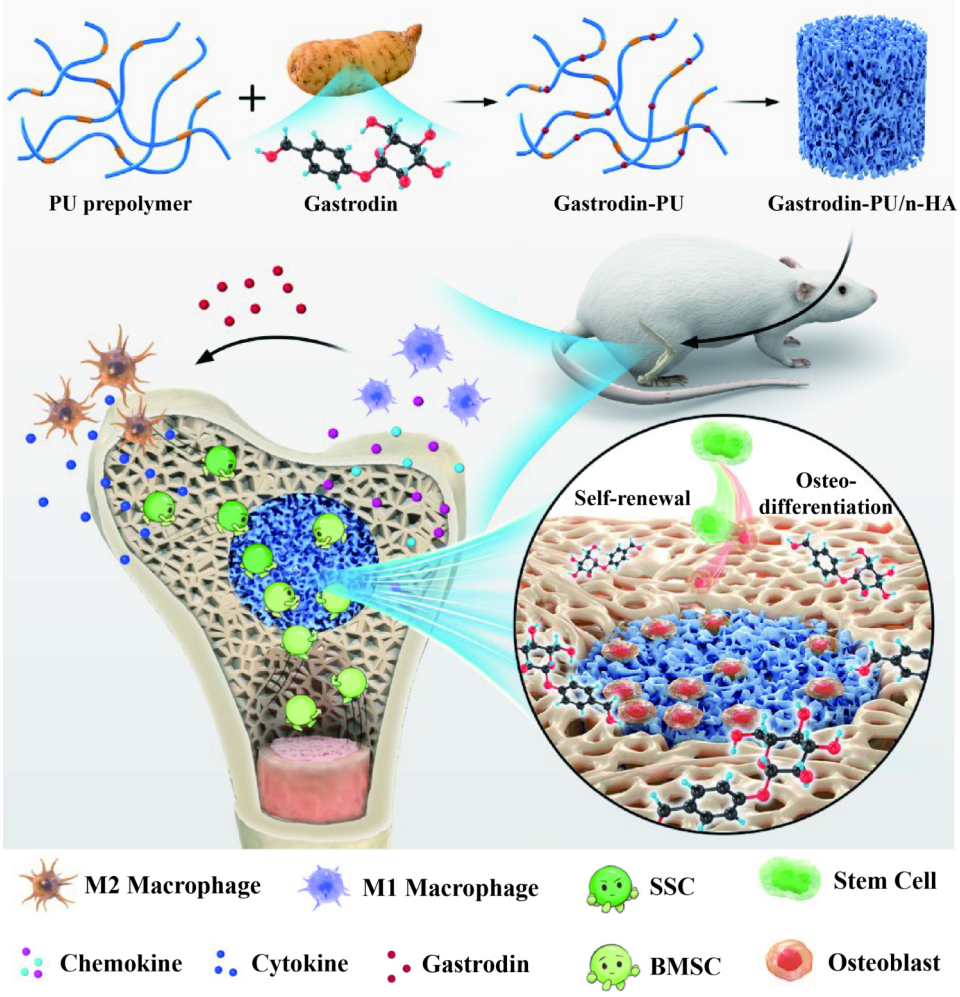

Scheme 1 Immuno-microenvironmentally optimized regenerative strategy for endogenous stem cells repairing bone defect: not only in favoring the recruitment of stem cells, but also in promoting their osteogenic differentiation in an ACD manner

Preparation and characterization of scaffolds

Fabrication of scaffolds Scaffolds were successfully synthesized through in situ foaming method according to our previously reported method [18]. In brief, PCL-2000 (30.00 g) and n-HA (11.40 g) were mixed in a 250 mL three-necked flask under nitrogen continuously and heated at 70 ℃, stirred with IPDI (9.17 g) for 2 h to obtain the prepolymer. Then 3.70 g of Lys-OEt·2HCl was used to extend the prepolymer for 2 h. After that, gastrodin of different contents (set as 0, 2, and 5 wt%) was added, followed by 1 mL $NaHCO_3$ solution. The resultant mixture was cured at 90 ℃ for subsequent use.

Characterization For the degradation and gastrodin release study, the scaffolds (~0.20 g) were immersed in 0.1 M and 0.5 M NaOH solution at 37 ℃ water bath, respectively. At 3/7, 1, 2, 3, 4, 5, 6, 7, 8 weeks, the residual weight and released gastrodin of each specimen were recorded. Micro-CT (Hiscan, China) and scanning electron microscopy (SEM) (Zeiss, Germany) were carried out to observe the microstructure of the scaffolds, and the porosity was quantified by dragonfly software (ORS, Canada). Mechanical properties were measured on a universal testing system (Instron, USA).

Surgical procedures

The scaffolds were cut into cylinder (Ø 3×3 mm) and sterilized by γ-ray irradiation with 15 kGy prior to use. The animal experiments were approved by the Institutional Animal Care and Use Committee of Kunming Medical University (China). Female Sprague-Dawley (SD) rats weighing 200 to 300 g were anesthetized with 3% sodium pentobarbital (30 mg/kg) and subjected to a standard bilateral ovariectomy (OVX) as described [28]. Three months after OVX, the osteoporotic rats were randomized into three groups: control, PU/n-HA, and 5% gastrodin-PU/n-HA. After exposure of lateral femoral condyle, a drill-hole defect with a diameter of 3 mm and a depth of 3 mm was created under abundant irrigation. The bone fragments were washed out from the cavity before the implantation of scaffolds, followed by repositioning and suturing of the tissue layers. The control group was operated without implantation of scaffolds. At postoperative days 3, 7, 14, and 28, rats were anesthetized for the peripheral blood harvesting. After sacrificing by cervical dislocation, bone marrow, and femur were also harvested for subsequent analysis.

Stem cells preparation

Bone marrow mesenchymal stem cells (BMSCs) were isolated from femurs according to our previously reported procedure [18] with minor revisions. At postoperative days 7 and 14, the femurs were soaked in 75% ethanol for 10 min and then washed with phosphate buffer saline (PBS, Solarbio, China). After both ends of the femur were removed, a disposable aseptic syringe drawing a complete medium consisting of α-minimum essential medium (α-MEM, Gibco, USA) supplemented with 10% fetal bovine serum (FBS, Gibco, USA) and 1% penicillin/streptomycin (Gibco, USA) was used to repeatedly wash the bone marrow cavity. About 4 mL of BMSCs suspension was obtained from two femurs of a rat, which was split into three portions: centrifuge tube (300 μL), T25 cell culture flask (300 μL), and culture plates (100 μL in 24-well plate and 200 μL in 6-well plate). Next, the BMSCs transferred to culture flasks and culture plates were further incubated at 37 °C, 5% CO_2, and 95% humidity. The complete medium was used for follow-up experiments and changed every 3 days unless otherwise stated.

For long-bone-derived skeletal stem cells (SSCs), femurs were dissected. After flushing out the bone marrow cells, the femurs with implants were then chopped into small pieces and digested by collagenase II (Sigma, U.S., 1 mg/mL) at 37℃ for 1 h. The digested cells were cultured in complete medium and allowed for functional assessment (See Scheme 2).

Endogenous stem cell recruitment

Flow cytometry (FC)

BMSCs in each tube were filtered with a 70 μm strainer to yield single cell suspensions. The cells were then incubated with red blood cell lysis buffer on ice, after which they were centrifugated and resuspended in FC sorting buffer (PBS with 10% FBS). Cells were stained with armenian hamster anti mouse/rat monoclonal antibodies CD29-APC (No.: 102215), mouse anti-rat monoclonal antibodies CD45-PE/CY7 (No.: 202213), and CD90-PE (No.: 205903) (Biolegend, USA) (1:200) according to the manufacturer's protocol. FC was performed using CyFlow® Space (Partec, Germany), and data analysis was conducted with FlowJo 10.5.3 software.

EdU incorporation assays

BMSCs were seeded in 24-well plates (100 μL/well) and maintained in culture. At 3 and 7 days, exponentially growing cells were stained with a Click-iT 5-ethynyl-2'-deoxyuridine (EdU) Alexa Fluor 594 Imaging Kit and nuclei were stained with Hoechest (Beyotime, China). Images were captured using a fluorescence microscope (Olympus, Japan). The numbers of EdU-positive cells were further counted by ImageJ software. The percentage of proliferating cells was calculated for each sample relative to the total number of Hoechest-positive cells.

Colony-forming unit fibroblast formation assay (CFU-F assay)

Self-renewal of BMSCs was assessed by a CFU-F assay. After being cultured in a 24-well plate (100 μL/well) for 7

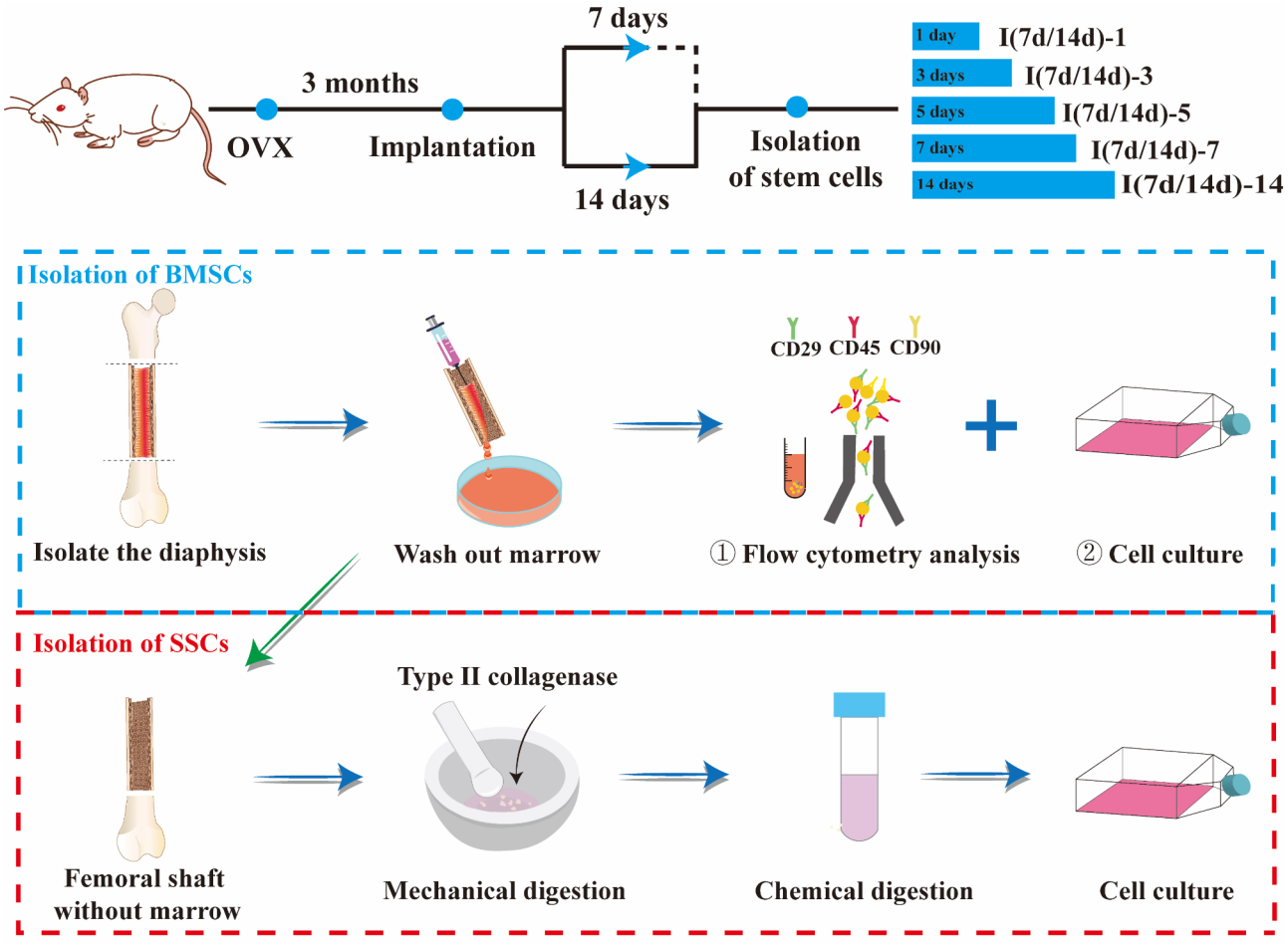

Scheme 2 Schematic illustration of the experimental outline. SD rats were subjected to a standard bilateral ovariectomy (OVX) and scaffolds were implanted into femoral condyle defect after 3 months. The stem cells were isolated and collected at 7 and 14 days, and further incubated for 1, 3, 5, 7, and 14 days for analysis

days, cells were fixed and stained with crystal violet solution (Beyotime, China).

Transwell-migration assay

A transwell chamber (24-well plate, 8 μm pore size, Corning Incorporated, USA) was used to evaluate the cell migration of retrieved scaffolds. The retrieved scaffolds were achieved from implants within osteoporotic bone defects or subcutaneous tissue after 7 and 14 days. Healthy 3-week-old rats served as donors of primary BMSCs, which were subcultured to the third passage (P3 BMSCs) according to the established procedure. Subsequently, 0.1 mL P3 BMSCs suspension (5×10^4 cells/mL) was added to the upper chamber. On the other hand, the retrieved scaffolds were placed in the lower chamber with 0.6 mL complete media. After 3 and 7-day incubation, the cells were fixed with 4% paraformaldehyde and stained with crystal violet. The non-invaded cells on the upside of the transwell were removed with a cotton swab, and the migrated cells to the underside were examined in three random fields under a light microscope. Meanwhile, the medium was collected and used for evaluation of secretion of SDF-1α and TGF-β cytokines with enzyme-linked immunosorbent assay (ELISA) kits (mlbio, China) following the manufacturer's guidance.

Functional assessment of stem cells

Mitochondrial activity of BMSCs

BMSCs were cultured with complete medium in 24-well plates for 7 and 14 days. At each time point, samples were stained with MitoTracker® Red CMXRos (Solarbio, China, No.: M9940) for active mitochondria. After fixation with 4% paraformaldehyde solution, the samples were stained with phalloidin (Solarbio, China, No.: CA1640) for actin and DAPI (Abcam, USA, No: ab104139) for nuclei. The mitochondrial membrane potential was detected using a probe 5,5',6,6'-Tetrachloro-1,1',3,3'-tetraethylbenzimidazolylcarbocyanine iodide (JC-1) assay kit (Solarbio, China, No.: J8030) according to the manufacturer's instructions.

For immunofluorescence (IF) staining, the wells were washed and fixed with 4% paraformaldehyde for 15 min at room temperature. The samples were then permeabilized in 0.1 % Triton X-100 for 20 min. Next, 5 % goat serum in PBS was added to the wells for 2 hours, followed by exposure to primary antibody cocktail, which was incubated overnight at 4 °C. The primary antibody involved mitochondrially encoded cytochrome C oxidase 2 (Mtco2), translocase of the outer mitochondrial membrane (TOM20), ATP synthase subunit alpha (ATP5A1), peroxisome proliferator-activated receptor-gamma coactivated 1α (PGC1α). Mtco2 (1:200), TOM20 (1:200), cocktail ATP5A1 (1:1000) and PGC1α (1:200) in 5% goat serum in PBS were used. The secondary antibodies were as follows: CoraLite488-conjugated goat anti-rabbit IgG (1:500, SA00013-2), CoraLite594-conjugated goat anti-rabbit IgG (1:200, SA00013-4), CoraLite594-conjugated goat anti-rabbit IgG (1:200, SA00013-4) and CoraLite488-conjugated goat anti-mouse IgG (1:500, SA00013-1). Mean optical density of the proteins was measured by Image J software. Each group comprised more than three wells, and each well was confirmed with cells collected from at least three separate animals. The related genes and proteins were further assessed as stated above.

Immunofluorescence staining of cells

BMSCs were seeded on coverslips in 24-well plates (100 μL/well) and cultured for 1, 3, 5, and 7 days. IF staining was carried out as indicated in the section IF staining of mitochondria. The following primary antibody cocktails in 5% goat serum in PBS were used: octamer-binding transcription factor 4 (OCT4) (1:200) and osterix (OSX) (1:200), β-catenin (1:2,000) and atypical protein kinase C (aPKC) (1:200). After rinsing with 0.05% PBST, the wells were incubated with secondary antibody cocktails for 2 h at room temperature. The secondary antibodies were as follows: CoraLite488-conjugated goat anti-rabbit IgG (1:500) and CoraLite594-conjugated goat anti-mouse IgG (1:200), CoraLite488-conjugated goat anti-mouse IgG (1:500) and CoraLite594-conjugated goat anti-rabbit IgG (1:200), of which the former corresponded to OCT4/OSX and the latter to β-catenin/aPKC cocktails. Finally, DAPI staining was performed for 2 h at room temperature. In parallel, the SSCs were also processed for the aforementioned IF staining.

Imaging and analysis of ACD process

All the imaging stacks were captured and processed using a confocal laser scanning microscope (CLSM) (Zeiss LSM 880, German) and Zen blue edition 3.3 software attached to the microscope. Briefly, z-stacks with 20 z-planes were acquired consecutively at a 1-μm z-step for each volume. Each z-stack was 3D-reconstructed and presented maximum intensity projections onto frontal X/Y, transverse (X/Z), and sagittal (Y/Z) planes. To calculate the proportion of the asymmetric stem cell division, 20 cell pairs were blindly chosen from each sample. The mean fluorescence intensity and distribution of the protein markers in paired daughter cells were measured, followed by normalization between the two newly formed daughter cells.

ACD-related gene expression

After the cells were subsequently cultured for 3 and 7 days, the ACD-related genes such as OCT4, OSX, β-catenin and aPKC were evaluated by reverse transcription quantitative polymerase chain reaction (RT-qPCR). The primer sequences are described in Table S1. Each sample was conducted in triplicates and repeated for three independent assays to achieve comparable results.

Endogenous new bone formation

Inflammatory/immune response analysis

At postoperative days 3, 7, 14, 28, the peripheral blood was collected in anticoagulant tubes for analysis using hematology analyzer (Sinnowa, China). The serum was derived from peripheral blood by centrifugation at 4000 rpm for 15 min. The content of inflammatory factors (Tumor Necrosis Factor-α (TNF-α) and interleukin-1β (IL-1β)) and reactive oxygen species (ROS) level in serum were detected by ELISA assay kit (Nanjing Jiancheng, China) according to the manufacturer's instructions. Tissue samples from the surrounding areas were collected and stored at -80 ℃ for the follow-up experiments. Total mRNA was extracted from bone tissue for analysis of macrophage phenotype biomarker genes, inducible nitric oxide synthase (iNOS) and arginase-1 (Arg-1).

Histological staining of tissue sections

The fixed samples were decalcified in 10% EDTA solution for 1 month, dehydrated through gradient ethanol, and then embedded in paraffin. Serial 5-μm thick sections were cut on a microtome (Leica Biosystems, Germany). The tissue sections were stained with Hematoxylin and eosin (H&E) (Solarbio, China), Masson's trichrome (Solarbio, China), and Movat's pentachrome (Solarbio, China) according to the supplied method by the manufacturer. Representative section images were captured with a light microscope (Olympus, Japan).

Immunohistochemistry staining of tissue sections

Tissue sections were incubated with a 3% H_2O_2 solution in methanol for endogenous enzyme quenching and treated with 0.1% trypsin-EDTA (Gibco, 25200056) to retrieve the antigen. After blocking with 5% goat serum for 1 h at 37 °C, the specimens were incubated overnight at 4 °C with primary antibodies against CD146 (1:200) for stem cell surface markers, BMP-2 (1:200) for

osteogenesis markers, Arg-1 (1:200) for an M2 marker, and iNOS (1:200) for an M1 marker, as listed in Table S2. The sections were washed with TBST before incubation with the secondary antibodies for 2 h. Sections were further incubated with secondary antibodies (Enhanced enzyme-labeled goat anti-mouse IgG polymer and Enhanced enzyme-labeled goat anti-rabbit IgG polymer), and then with DAB reagents (Diaminobenzidine tetrahydrochloride staining, Boster Biological Technology Co. Ltd., China), followed by counterstaining with hematoxylin. The sections were mounted prior to imaging. Brown staining localization within the defects indicated positive expression of the biomarkers under an optical microscope. The positive cell ratio of the proteins was calculated by software Image J and GraphPad Prism v8.0. Each type of staining was confirmed in tissues from more than three separate rats.

Micro-computed tomography (micro-CT) analysis

Four weeks after implantation, femurs were collected and fixed in 4% paraformaldehyde for 3 days. The fixed samples were scanned using micro-CT (Pingseng scientific, China) at a resolution of 7.5 μm with a voltage of 90 kV and a current of 60 μA. During the reconstruction, a threshold between 1000 and 3000 was applied to discriminate the bone tissue, and a threshold between 600 and 1000 was applied to discriminate the scaffold. Three-dimensional (3D) and two-dimensional (2D) analysis were performed using Avatar3 software attached to the micro-CT. 3D reconstructed structures of the distal femur were acquired from the segmented dataset for visual inspection. For the quantitative evaluation of osteogenesis within defects, a consistent cylinder at a diameter of 2.5 mm and a height of 2.5 mm was chosen as the region of interest (ROI) to represent remnant scaffold and regenerated bone. To study the effect of the scaffolds on adjacent bone loss, another rectangular ROI ($0.5\times0.5\times2$ mm^3) adjacent to the defect, which was 1.5 mm away from the epiphyseal growth plate, was also selected and analyzed. The structural parameters of new bone and trabecular bone, including bone mineral density (BMD), trabecular bone volume fraction (BV/TV), trabecular number (Tb.N), trabecular thickness (Tb.Th), and trabecular separation (Tb.sp), were calculated through the micro-CT scans.

Statistical analysis

Data were reported as means ± standard deviation (SD). One-way analysis of variance (ANOVA) was applied for statistical comparisons among more than two groups, and a t-test was used for statistical comparisons between two groups. All statistical analyses were performed using GraphPad Prism v8.0.2. Statistical significance was accepted at $P<0.05$.

Results

Characterization of gastrodin-functionalized scaffolds

Gastrodin was chemically grafted onto a polyurethane matrix, which degraded in a gradient, to achieve consistent release of gastrodin and increase its therapeutic efficiency. The degradation behavior of the scaffolds in 0.1 M NaOH solution showed that the 5% gastrodin-PU/n-HA scaffold degraded substantially by losing more than 24.06% of its original weight within the first 3 weeks. This was followed by higher degradation rates until residuum was hardly distinguishable at 8 weeks. In contrast, the 2% gastrodin-PU/n-HA scaffold showed a slower degradation rate, while PU/n-HA maintained a much more stable structure (Fig. 1A). Meanwhile, a similar degradation pattern was observed in the 0.5 M NaOH solution and the mass loss was significantly increased over a period of 3 weeks. In addition, it was found that gastrodin released from both 2% and 5% gastrodin-PU/n-HA scaffolds increased gradually with time. Gastrodin released from 5% gastrodin-PU/n-HA appeared to be higher than that from 2% gastrodin-PU/n-HA, yet no significant difference was observed between both groups over a period of 3 weeks. However, the release of gastrodin from 5% gastrodin-PU/n-HA in 0.1 M NaOH solution undertook a relatively steady and sustained release kinetic by showing a durable release for as long as 8 weeks. The degradation may be associated with highly interconnected porous structure. As exhibited in micro-CT and SEM, the pore size ranged from 200 to 800 μm (Fig. 1B) and porosity was close to 60% (Fig. 1C). By adding gastrodin proportion, the compression strength of 5% gastrodin-PU/n-HA (5.55 ± 0.79 MPa) was markedly enhanced, which was higher than 2% gastrodin-PU/n-HA (2.89 ± 0.81 MPa) and PU/n-HA group (1.87 ± 1.10 MPa) (Fig. 1D). Similar results were also found in elastic modulus. Therefore, we believe that 5% gastrodin-PU/n-HA with adequate gastrodin delivery and mechanical strength is a candidate scaffold of choice for further experimentation.

Scaffold promotes M2 macrophage polarization in endogenous bone regeneration

Whether the scaffold can provide an appropriate microenvironment is vital in determining its quality and efficiency for endogenous bone regeneration. PU/n-HA and 5% gastrodin-PU/n-HA were implanted, respectively, into the condyles of femur in osteoporotic rats. Results by ELISA kit showed a large amount of pro-inflammatory proteins in the serum of control, e.g., TNF-α and IL-1β. However, the expression levels of pro-inflammatory proteins were decreased in PU/n-HA group and were the lowest in 5% gastrodin-PU/n-HA group in the early stage of inflammation (Fig. 2A and B). The inflammation was further attenuated with prolonged implantation time. The expression changes of ROS were in tandem with the

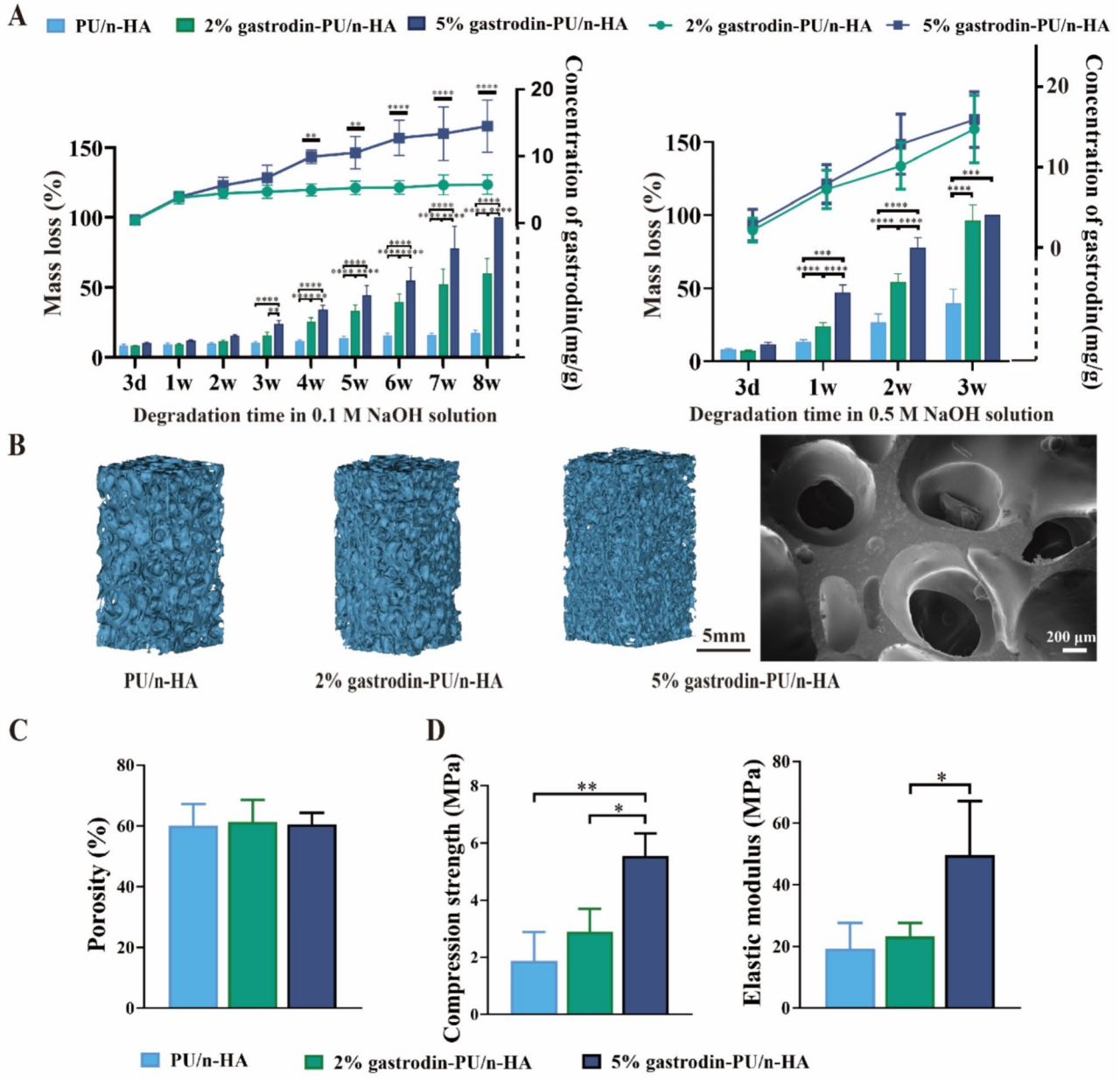

Fig. 1 Characterization of porous scaffolds. (**A**) In vitro degradation and gastrodin release profiles in 0.1 and 0.5 M NaOH solution ($n=4$). (**B**) Microstructure of scaffolds was observed by Micro-CT and SEM. (**C**) Porosity of scaffolds. (**D**) Mechanical properties including compression strength and elastic modulus. Error bars represent the standard deviation from the mean ($n=3$). ****$p<0.0001$; ***$p<0.001$; **$p<0.01$; *$p<0.05$

proinflammatory proteins. Thus, the ROS level in control group was higher than that in PU/n-HA group, more so than in 5% gastrodin-PU/n-HA group (Fig. 2C).

As shown by IHC staining (Fig. 2D and E), 7 days after 5% gastrodin-PU/n-HA implantation, only moderate inflammatory protein iNOS staining (M1 macrophage) was detected within the scaffolds. By 14 days post-implantation, the expression was minimally detectable. On the other hand, intense staining for the anti-inflammatory marker Arg-1 (M2 macrophage) was detected at both 7 and 14 days. In the control group without implants, the bone defects showed positive iNOS expression at 7 and 14 days, indicating an excessive inflammatory microenvironment. In the PU/n-HA group, there was evidence of transition from M1 to M2 macrophages labeled by their respective markers. Nonetheless it was inferior to 5% gastrodin-PU/n-HA group which showed a higher incidence of M2 macrophages. Detection of related genes from tissues in scaffold and surrounding bone further confirmed that Arg-1 in the 5% gastrodin-PU/n-HA group was higher than that in the PU/n-HA and control groups at both time points. As opposed to

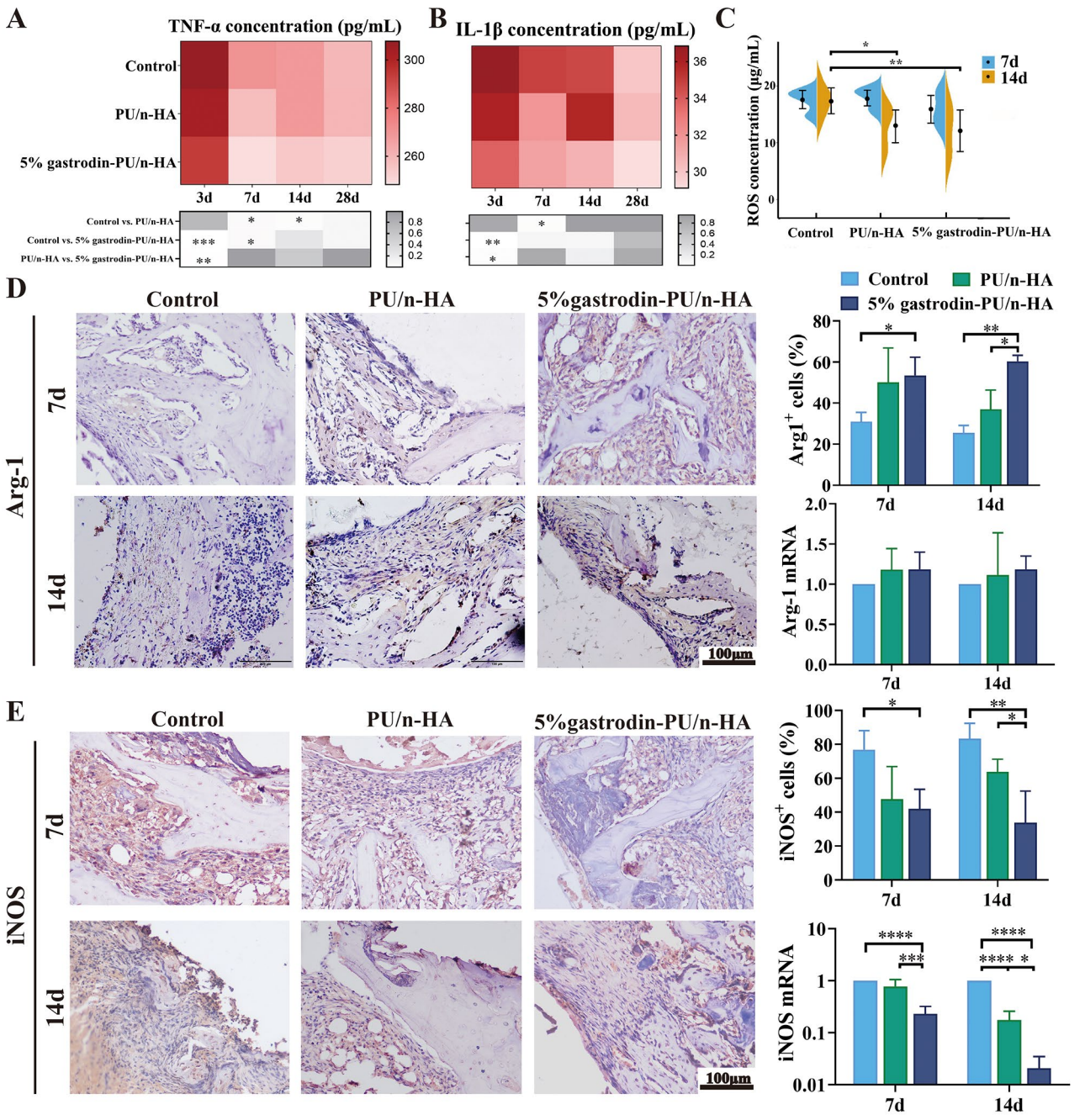

Fig. 2 In vivo immune response of scaffolds in femoral condyle defect model at postoperative days 3, 7, 14, and 28. (**A**, **B**, **C**) The plasma levels of TNF-α (A), IL-1β (B), and ROS (C) ($n=6$). (**D**) Representative IHC staining of Arg-1 (left panel) and semiquantification of positively stained cells (upper right panel), and relative gene mRNA expression of tissues (lower right panel) at 7 and 14 days. (**E**) Representative IHC staining of iNOS (left panel) and semiquantification of positively stained cells (upper right panel), and relative gene mRNA expression of tissues (lower right panel) at 7 and 14 days. Error bars represent the standard deviation from the mean ($n=3$). ****$p<0.0001$; ***$p<0.001$; **$p<0.01$; *$p<0.05$

this, iNOS expression in 5% gastrodin-PU/n-HA group was attenuated. Taken together, it can be confidently concluded that compared with PU/n-HA, 5% gastrodin-PU/n-HA can exert a more potent anti-inflammation by promoting M2 macrophage polarization. This corroborates with our previous findings.

Scaffold recruits endogenous stem cells in bone regeneration

Considering stem cell-dependent bone growth and repair, we hypothesized that homing host stem cells to defect site would enhance bone healing. IHC staining showed that the recruited cells expressed CD146 (the surface

markers for stem cells) at both time points (Fig. 3A). A higher percentage of $CD146^+$ cells was observed in the implant groups in comparison with the control group at 7 days. Semiquantitative analysis results confirmed the obviously enhanced positive expression. Compared with PU/n-HA, therefore, 5% gastrodin-PU/n-HA was capable of recruiting more stem cells. This lasted up to 14 days, suggesting effective mobilization of endogenous stem cells to reach regenerative site, which was conducive for new bone formation. We next analyzed the populations of BMSCs isolated from implanted femurs at post-surgery days 7 (I(7d)) and 14 (I(14d)) using FC (Fig. 3B). There was no significant difference in absolute cell numbers between the control and PU/n-HA group. However, the absolute numbers of BMSCs in 5% gastrodin-PU/n-HA group were significantly increased at post-surgery days 7 and 14. They were significantly higher than that in the control and PU/n-HA groups at both time points. The migration efficiency of BMSCs in response to the retrieved implants was next studied *via* transwell assay. As shown in Fig. 3C, the crystal violet staining was all enhanced in implant groups after culturing for 3 (I(7d)-3) and 7 (I(7d)-7) days, of which 5% gastrodin-PU/n-HA was better than PU/n-HA group, suggesting optimal migration capacity of BMSCs by 5% gastrodin-PU/n-HA-optimized microenvironment. There was less migration in control after culturing for 3 (I(7d)-3), and even less so at 7 (I(7d)-7) days. Consistent with the migration ability, 5% gastrodin-PU/n-HA showed a higher level of chemokines compared to other groups (Fig. 3D). Scaffolds were also subcutaneously transplanted and then retrieved at 7 days (Fig. 3E). The transwell assay showed that the BMSCs had migrated to the lower chamber after culturing for 3 days ((I(7d)-3) but the migration was moderately reduced at 7 days ((I(7d)-7) in 5% gastrodin-PU/n-HA group. The expressions of SDF-1 and TGF-β in the supernatant exerted greater migration activity of BMSCs in 5% gastrodin-PU/n-HA group than those derived from PU/n-HA group (Fig. 3F). This might have altered the resident-stem-cell behavior *via* specific modulation in their regenerative niche.

Scaffold-optimized microenvironment activates BMSCs

To assess proliferative activity, BMSCs collected at post-surgery days 7 and 14 were respectively cultured for 3 and 7 days. Most BMSCs entered the cell division cycle, as evidenced by the incorporation of EdU (Red fluorescence). Compared to the control, the percentage of EdU-positive cells increased in the PU/n-HA groups, notably in the 5% gastrodin-PU/n-HA group. Although BMSCs collected at post-surgery day 14 presented a consistent upward trend comparable to post-surgery day 7, the number of EdU-positive cells did not increase, further indicating a decrease in dividing cells. These results suggested that 5% gastrodin-PU/n-HA not only could recruit more BMSCs, but it could also maintain the maximum proliferation of stem cells in the early stage (Fig. 4A and B). Thus, increased proliferative and chemotactic activity of BMSCs induced by scaffolds contribute to the functional stem and progenitor cell response.

By CFU-F assay, we next assessed whether scaffolds, as the extrinsic stimulus, would have any effects on colony formation of recruited endogenous stem and progenitor cells. After cultured for 7 days, BMSCs at both time points all formed abundant CFU-Fs being more pronounced in 5% gastrodin-PU/n-HA group, suggesting powerful cellular self-renewal ability (Fig. 4C). When the BMSCs were further cultured in an osteogenic induction medium for 7 days, some osteogenic genes, such as OSX, BMP-2 and runt-related transcription factor 2 (Runx2), were vigorously expressed in the 5% gastrodin-PU/n-HA group, and noticeably more intense than those in the PU/n-HA and control groups. In line with RT-qPCR results, the cells in the 5% gastrodin-PU/n-HA group showed highly positive staining for ALP on day 7, as well as mineralized nodules that were positive for alizarin red S staining on day 21 compared with that in the PU/n-HA group, and the control group with the last-mentioned being the lightest in staining (Fig. S1). Taken together, it is concluded that the microenvironment remodeled by the 5% gastrodin-PU/n-HA scaffold can contribute to the osteo-differentiation response in recruited BMSCs.

As mitochondria are the main source of energy for cells, the regulation of mitochondria dynamics and function is essential for successful differentiation of BMSCs. At 7 days post-surgery, the BMSCs were cultured for further 7 days. Images of single cell exhibited a smaller area of cytoskeleton assembly in the control group but as flat lamellipodia in the PU/n-HA group. The BMSCs in treated with the 5% gastrodin-PU/n-HA group showed long extending and branching cellular pseudopods. MitoTracker Red staining showed a significant increase in mitochondrial membrane potential (MMP) in the 5% gastrodin-PU/n-HA group when compared with that in other groups. A noteworthy feature was the relatively higher level of MMP in PU/n-HA than in the control (Fig. 4D). Moreover, the expression of TOM20 (Fig. 4E) and Mtco2 (Fig. 4F) was greatly improved in the 5% gastrodin-PU/n-HA group. Enhanced ATP5A1 and PGC1α colocalization staining (Fig. 4G) further confirmed the increase in mitochondrial mass. Interestingly, the mitochondria were mainly clustered around the nucleus in the control and PU-n/HA groups, but they tended to be more uniformly distributed throughout the cytoplasm in the 5% gastrodin-PU/n-HA group. It is relevant to note that BMSCs undergoing osteo-differentiation showed mainly slender mitochondria. The mitochondrial-to-cytoplasm area ratio was increased during osteo-differentiation in

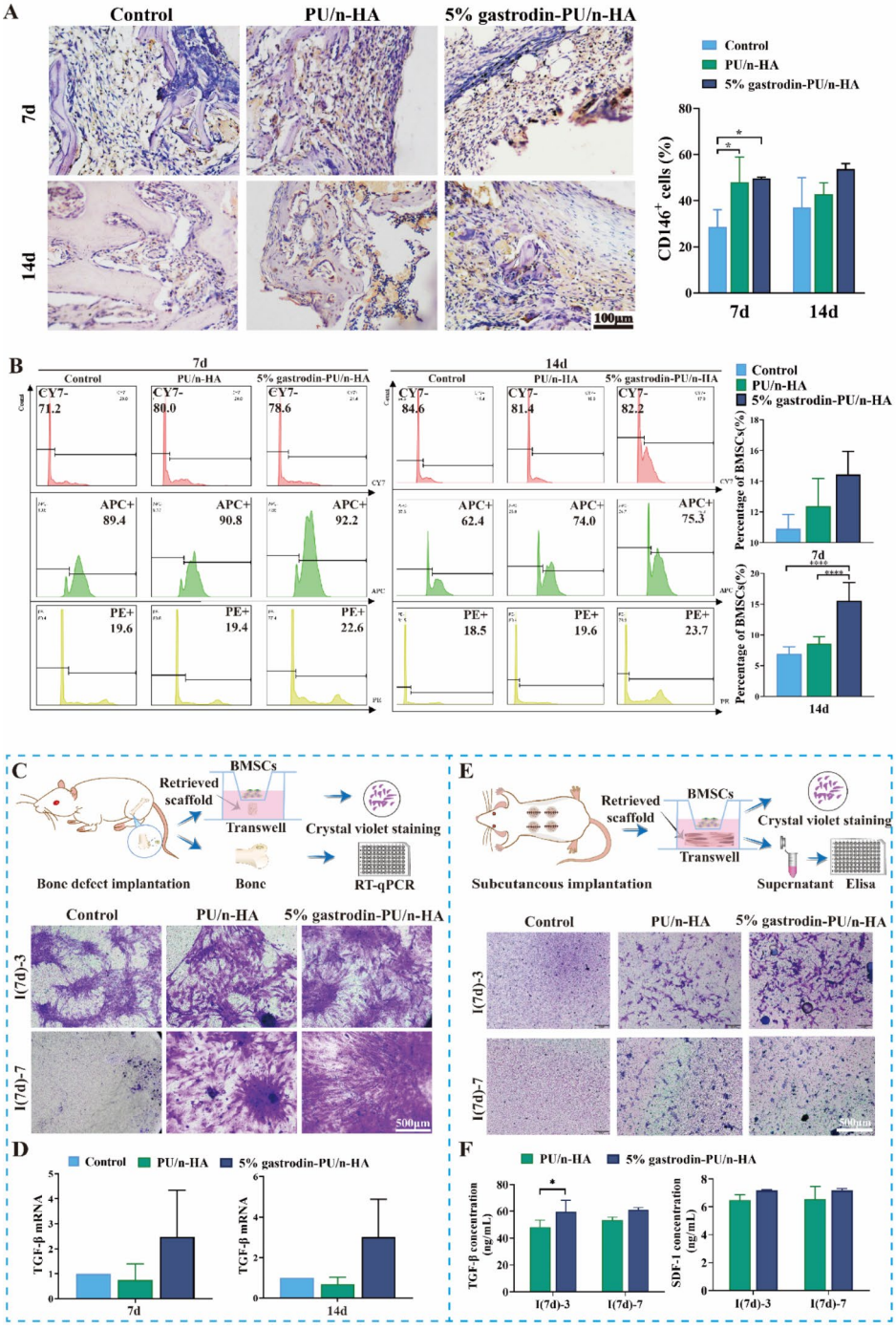

Fig. 3 Endogenous stem cell recruitment in response to scaffolds after implantation for 7 and 14 days. (**A**) Representative IHC staining of CD146 and semiquantification of positively stained cells. (**B**) FC analysis of $CD29^{+}/CD45^{-}/CD90^{+}$-cells in diaphysis marrow and quantitative histogram of the percentage of recruited BMSC-like cells. (**C**) Schematic depiction of in vitro BMSCs recruitment in transwell by incubating retrieved scaffold that was implanted into femoral condyle defect for 7 days. Migrated cells were stained by crystal violet at 3 and 7 days. (**D**) The expression of TGF-β mRNA of bone tissue at postoperative days 7 and 14. (**E**) Schematic depiction of in vitro BMSCs recruitment in transwell by incubating retrieved scaffold that was subcutaneously implanted for 7 days. Migrated cells were stained by crystal violet at 3 and 7 days. (**F**) Expression levels of chemokines in supernatant. Error bars represent the standard deviation from the mean ($n = 3$). $^{****}p < 0.0001$; $^{*}p < 0.05$

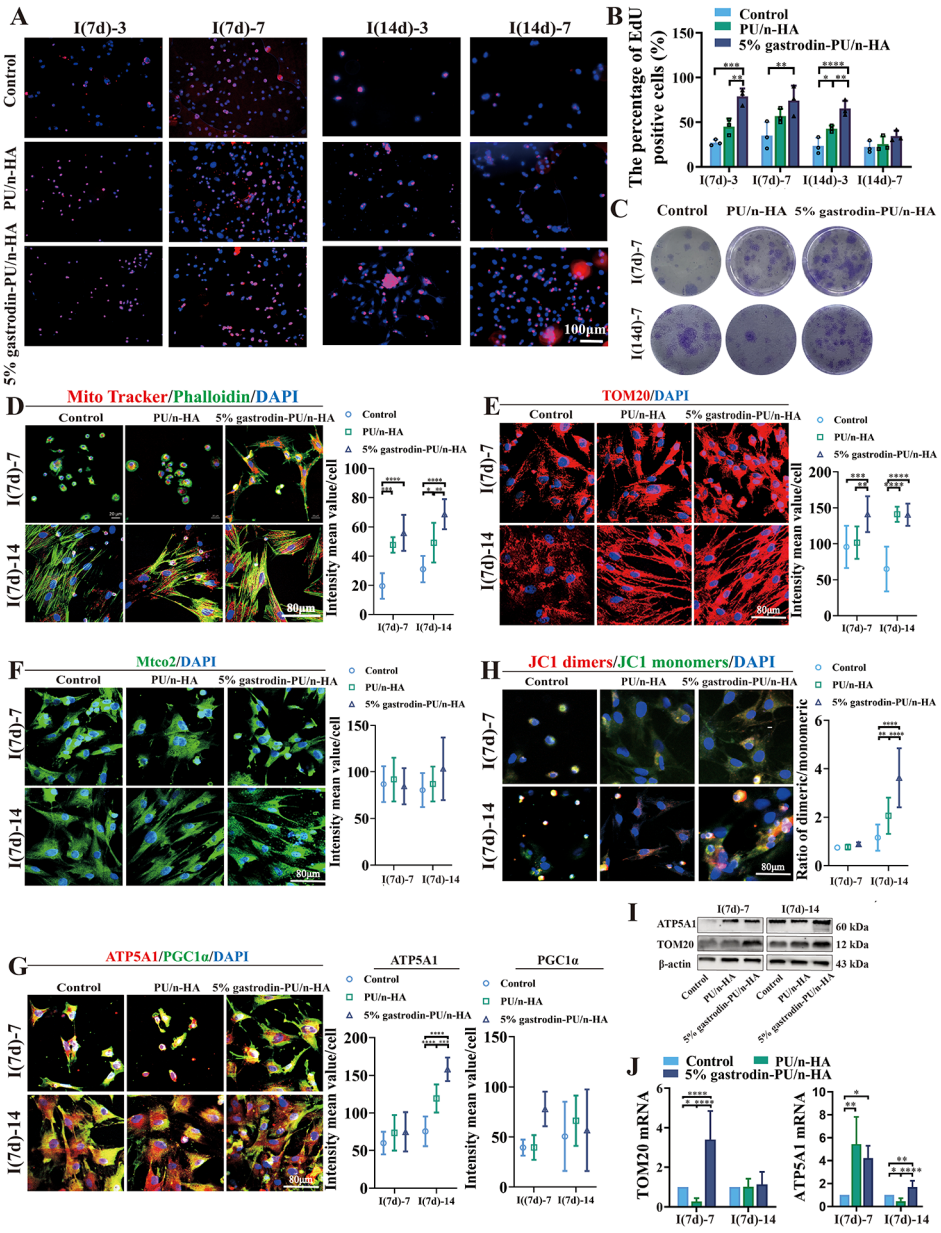

Fig. 4 Proliferation and mitochondrial activity in BMSCs derived from defective SD rats which were treated with scaffolds for 7 (I(7d)) and 14 (I(14d)) days. (**A**) EdU staining when further cultured for 3 and 7 days. (**B**) The semiquantitative histogram of the percentage of EdU positive cells ($n=3$). (**C**) Colony formation when further cultured for 7 days. (**D-H**) Representative confocal microscopy images (left panel) of (D) co-expressing a Mito-Tracker (red) and Phalloidin (green), (E) TOM20 (red), (F) Mtco2 (green), (G) ATP5A1 (red) and PGC1α (green), as well as semiquantitative analysis of the optical density (right panel), and (H) JC1 monomer (green) and JC1 dimer (red) with nuclei (blue). The ratio between the red and green fluorescence of cells loaded with JC-1 represents the mitochondrial membrane potential. (**I-J**) ATP5A1 and TOM20 expression as measured by western blotting (I) and RT-qPCR ($n=3$) (J). Error bars represent standard deviation from mean ($n=10$). ****$p<0.0001$; ***$p<0.001$; **$p<0.01$; *$p<0.05$

5% gastrodin-PU/n-HA relative to that of undifferentiated cells in other groups. The increase was more in BMSCs harvested from post-surgery day 14 (Fig. 4H). The green fluorescence (monomers) of JC-1 gradually became red (dimers) in the course of differentiation, indicating increased mitochondrial biogenesis. It is worth noting that TOM20 and ATP5A1 proteins were increased in the 5% gastrodin-PU/n-HA group, although the differences did not reach statistical significance among all groups according to western blotting analysis (Fig. 4I). Using RT-qPCR with specific primers, TOM20 was observed to be activated by 5% gastrodin-PU/n-HA. ATP5A1 showed a moderate decline in the 5% gastrodin-PU/n-HA group compared with that in the PU/n-HA group at 7 days, followed by a significant increase at 14 days (Fig. 4J). Accumulating evidence suggests that 5%

gastrodin-PU/n-HA boosts mitochondriogenesis and regulates the homeostasis of the mitochondrial network to meet the increased energy demand for differentiation of stem cells' biological behavior.

Asymmetric cell division of BMSCs in scaffold-optimized microenvironment

To understand how the scaffold might affect the local microenvironment and division mode of recruited stem cells, BMSCs were seeded and cultured for 1, 3, 5, and 7 days. Expression of OSX (an osteoblast-specific transcription factor) and OCT4 (a key transcription factor in maintaining the self-renewal of stem cells) was analyzed. Co-localized IF staining showed that BMSCs in all groups continued to proliferate over the extended period (Fig. 5A). Over the first day, viable cells exhibited a round cellular outline in both control and PU/n-HA groups, whereas some cells in the 5% gastrodin-PU/n-HA group were extended, showing a larger cell area. From day 3 to day 7, more active BMSCs with long extending processes were detected in the 5% gastrodin-PU/n-HA group compared with other groups. Concomitantly, the cell number was increased. Of note, OCT4 was vigorously expressed in the 5% gastrodin-PU/n-HA group as early as day 1. OCT4, however, was weakly expressed in the control and PU/n-HA groups. Meanwhile, the incidence of OCT4-positive cells was further increased in the 5% gastrodin-PU/n-HA group compared with the other groups on day 3, even though the positive cells in other groups were moderately increased. The continued elevation in stem cell expression in the 5% gastrodin-PU/n-HA group on days 5 and 7 indicated active stemness and pluripotency compared with the PU/n-HA group and control group. Along with OCT4, the osteo-differentiation marker OSX was also analyzed. The number of OSX^+ cells in the 5% gastrodin-PU/n-HA group was significantly higher than that in the PU/n-HA group, with the control group showing the least number of positive cells (Fig. 5B). The increase in OSX^+ cells was positively correlated with the culture period. A similar trend was also observed in BMSCs derived from SD rats which was treated with the scaffold for 14 (I(14d)) days (Fig. S2). When considering the fate of stem cells, as shown in Fig. 5A, some of cell pairs generated one cell expressing OSX while the other maintained OCT-4 expression, suggesting that asymmetrical division had occurred in a subset of the BMSCs. Of 20 cell pairs scrutinized, those undergoing asymmetric division made up the highest percentage in the 5% gastrodin-PU/n-HA group, peaking at the 5th day.

We further visualized two categories of dividing cells in representative 5% gastrodin-PU/n-HA group using 3D imaging. In individual dividing BMSC, OSX was enriched to one side of the cell, while OCT4 was unequally distributed on both sides of the cytoplasm with maximum bias to one side (Fig. 5C and Movie S1). Note that generating the daughter cells differed in size based on the intensity and distribution of the markers: those that associated with OSX were smaller, and those that mainly expressed OCT4 were comparatively larger (Fig. 5C). The findings were consistent with the requirement for cell polarity and asymmetric division potential adapting to size changes. The RT-qPCR analysis of OSX and OCT4 supported the observation that co-expression of osteo-differentiation and stem cell markers was markedly elevated in the 5% gastrodin-PU/n-HA group compared with the other groups at either time point (Fig. 5D).

Cell fate markers in dividing BMSCs

A significant amount of effort has been devoted toward understanding the underlying molecular mechanism of aforementioned cell fate. Stem cells undergoing asymmetric cell division often require compartmentalization of the polarity proteins to one side of the cell. aPKC, a polarity protein implicated in ACD, was highly expressed in cells of 5% gastrodin-PU/n-HA group and peaking at day 5. Another polarity protein, β-catenin, coincided with that of aPKC distribution. In contrast, in PU/n-HA, both expression of polarity proteins was attenuated and was weakest in control group (Fig. 6A). Next, we studied the correlation between cell number and polarity protein level. It was observed that polarity protein was noticeable when cells proliferated over a prolonged culturing period. In a single dividing BMSC, the aPKC and β-catenin proteins were mainly co-enriched in one half of the paired daughter cells, wherein β-catenin exhibited minimal bias to other side (Fig. 6B and C). In symmetric divisions, both proteins were distributed throughout the cell with minimal bias to either side (Fig. S3). Thus, one-sided localization of proteins in 5% gastrodin-PU/n-HA group effectively induced the asymmetric distribution of the Par complex in some dividing cells to discriminate the fates of daughter cells. This was further supported by the increased gene expressions of aPKC and β-catenin (Fig. 6D).

Asymmetric cell division of SSCs in scaffold-optimized microenvironment

A similar type of lineally related skeletal stem cells (SSCs) that possess self-renewal and multipotency, may also prospectively contribute to functions of bone. We therefore also cultured the SSCs isolated from femurs with implants to examine the distribution of OSX and OCT4 expression during cell division (Fig. 7A). After culturing for 1 day, the 5% gastrodin-PU/n-HA group showed a higher proportion of OSX positive cells in comparison with PU/n-HA group. OCT4 positive cells were also observed in both groups. In the control group, rarely osteogenesis-related OSX positive cells were identified.

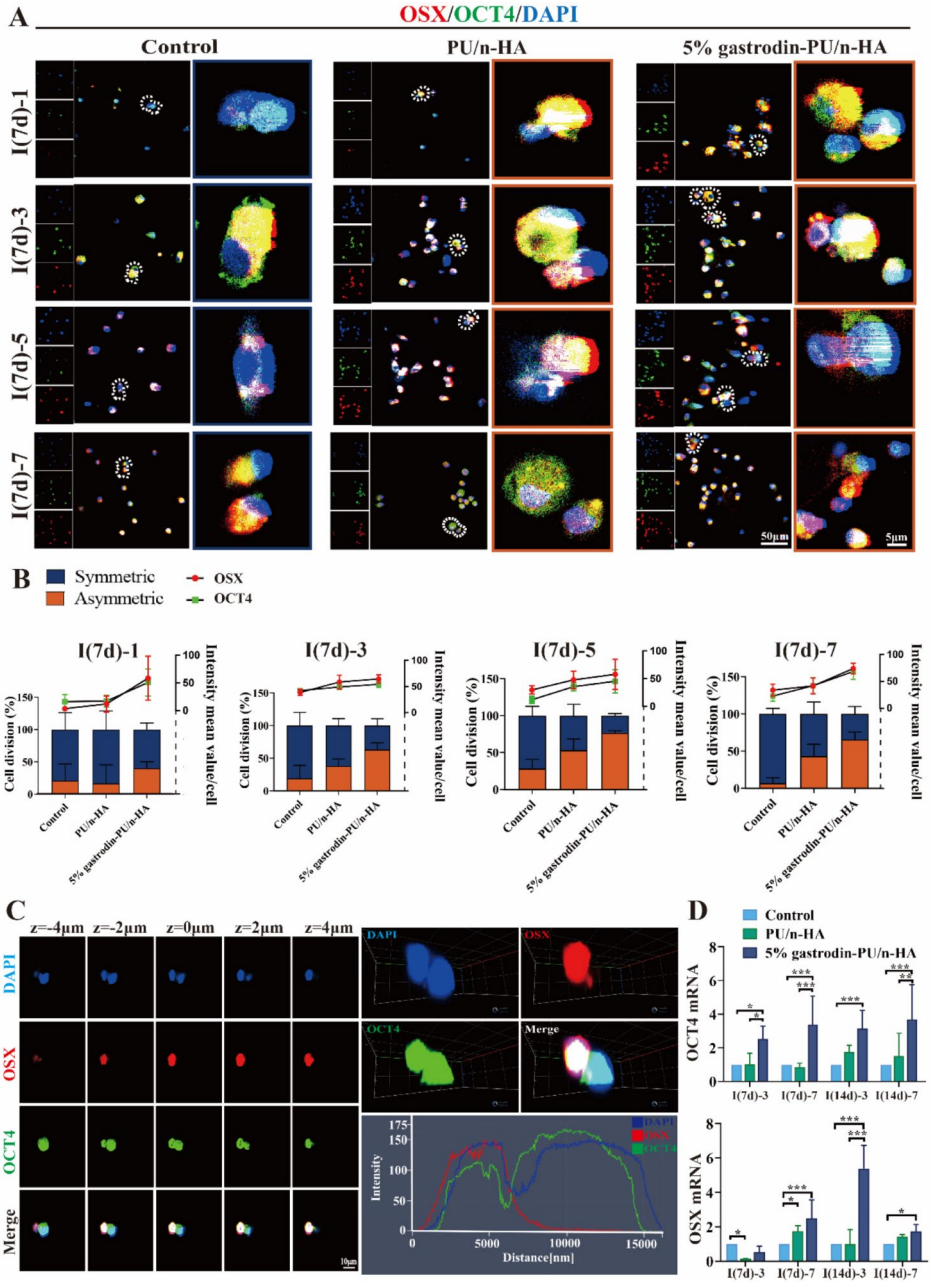

Fig. 5 Asymmetric cell division in BMSCs derived from defective SD rat which was treated with scaffold for 7 (I(7d)) and 14 (I(14d)) days. (**A**) Representative confocal microscopy images of co-expressing an osteogenic (OSX, red) and stem cell marker (OCT4, green), and DAPI (blue) in paired daughter cells when further cultured for 1, 3, 5, and 7 days. (**B**) Both OSX and OCT4 appeared asymmetrically versus symmetrically segregated into the daughter cells. Cell division and optical density were calculated from 20 cell pairs ($n=20$). (**C**) Consecutive images of confocal z planes (left panel), 3D reconstructions of ACD (upper right panel), and Z-plot of optical density (low right panel). (**D**) Relative gene levels of OSX and OCT4. Error bars represent standard deviation from mean ($n=3$). ***$p<0.001$; **$p<0.01$; *$p<0.05$

However, occasional OCT4 positive cells were detected. Over time, both OCT4 and OSX IF in all groups was further enhanced, accompanied by cell proliferation. The expression increased pattern bears resemblance to that the BMSCs division. Thus, with respect to cell division both BMSCs and SSCs showed stem and differentiation marker distribution to either side between the two cell halves or cell pair and this had allowed them to polarize (Fig. S4).

The co-expression of aPKC and β-catenin, albeit at different levels, was in agreement with the results of OSX and OCT4 labeling (Fig. 7B). The 5% gastrodin-PU/n-HA group exhibited the most potent aPKC expression. Indeed, its facilitating effect on both osteo-differentiation

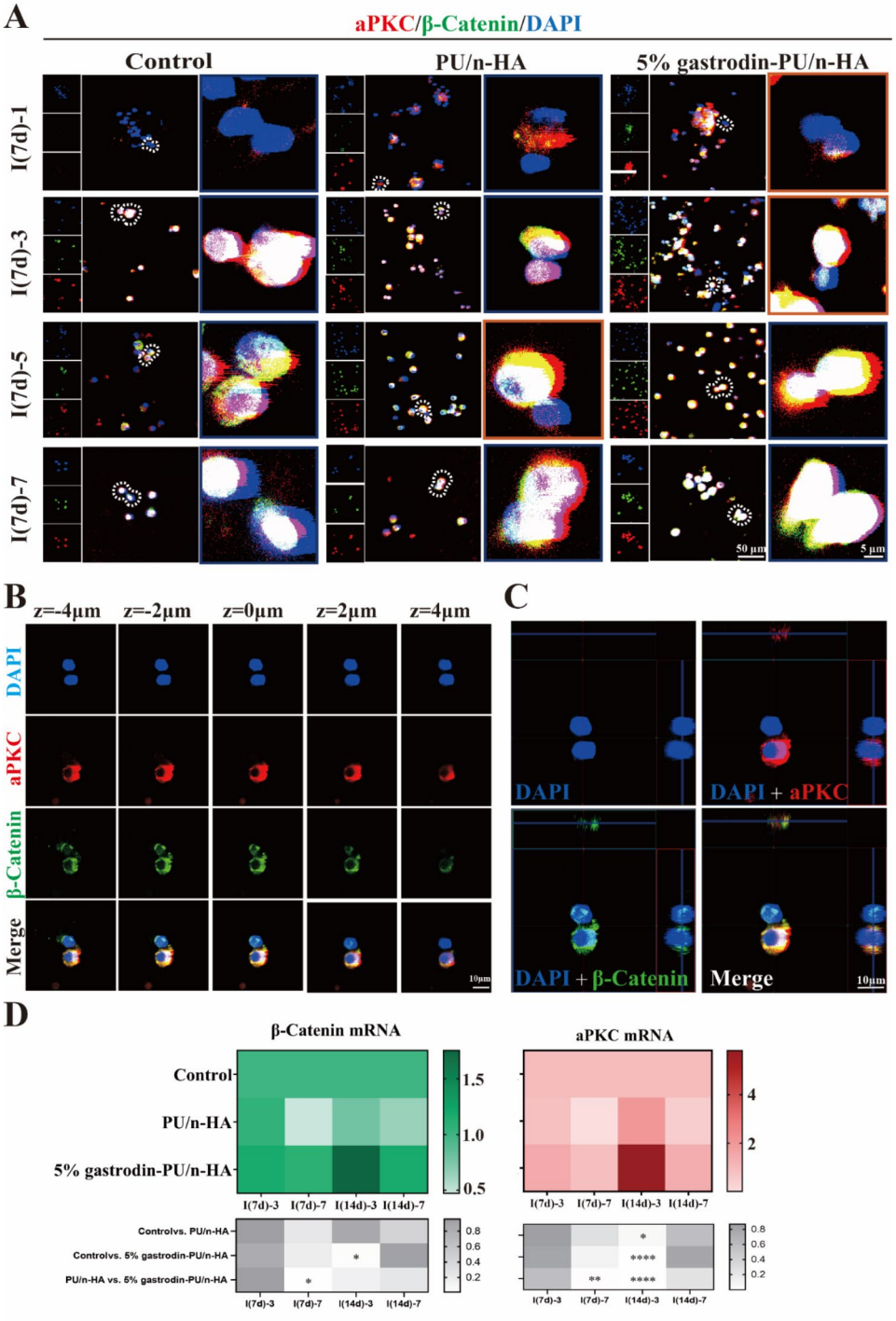

Fig. 6 Microenvironmentally optimized scaffold induced asymmetric distribution of cell fate markers in BMSCs. (**A**) Representative confocal microscopy images of co-expressing aPKC (red) and β-catenin (green), and DAPI (blue) in paired daughter cells when further cultured for 1, 3, 5, and 7 days. (**B**) Representative confocal z planes of typical asymmetric cell division. (**C**) 3D reconstructions of ACD. (**D**) Relative gene expression of β-catenin and aPKC. Error bars represent standard deviation from mean ($n = 3$). ****$p < 0.0001$; **$p < 0.01$; *$p < 0.05$

and polarization function was evidently stronger than PU/n-HA group. Also, β-catenin was enriched in the 5% gastrodin-PU/n-HA group peaking at the 5th day; it is mainly associated with the stem cell maintenance. A more robust activation as observed in 5% gastrodin-PU/n-HA in comparison with other groups, confirms its effect on higher ACD efficiency. The significant differences in the increase in relative expression of OSX, OCT4, aPKC, and

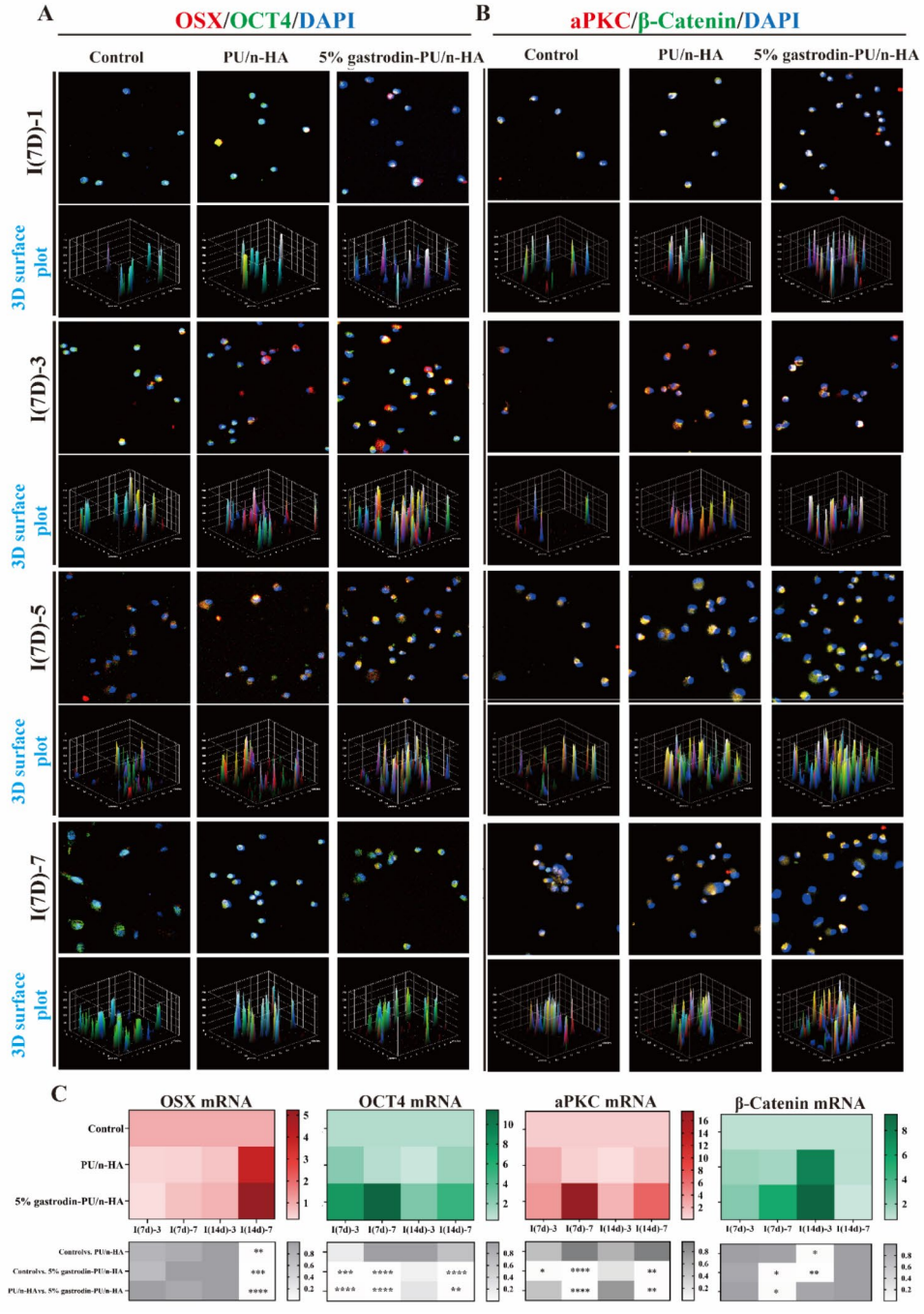

Fig. 7 Asymmetric cell division in SSCs derived from defective SD rat which was treated with scaffold for 7 (I(7d)) and 14 (I(14d)) days. (**A-B**) Representative confocal microscopy images of co-expressing (A) OSX (red) and OCT4 (green), and (B) aPKC (red) and β-catenin (green) in dividing cells when further cultured for 1, 3, 5, and 7 days. (**C**) Relative gene-expression activity of OSX, OCT4, aPKC, and β-catenin. Error bars represent standard deviation from mean ($n = 3$). ****$p < 0.0001$; ***$p < 0.001$; **$p < 0.01$; *$p < 0.05$

β-catenin by 5% gastrodin-PU/n-HA had gained further support by RT-qPCR analysis (Fig. 7C). The results demonstrated that the recruited SSCs expressed both stem and osteo-differentiation markers in 5% gastrodin-PU/n-HA after implantation for 7 and 14 days.

Ingrown and adjacent bone analysis of scaffold implants

Histological staining of tissue sections provides details on new bone formation at the scaffolds after implantation for a relatively short time. H&E staining in Fig. 8 showed little tissue infiltrated at 14 days, and only a small amount of newly formed connective tissue appeared in the defect boundary in the control group at 28 days. There was a

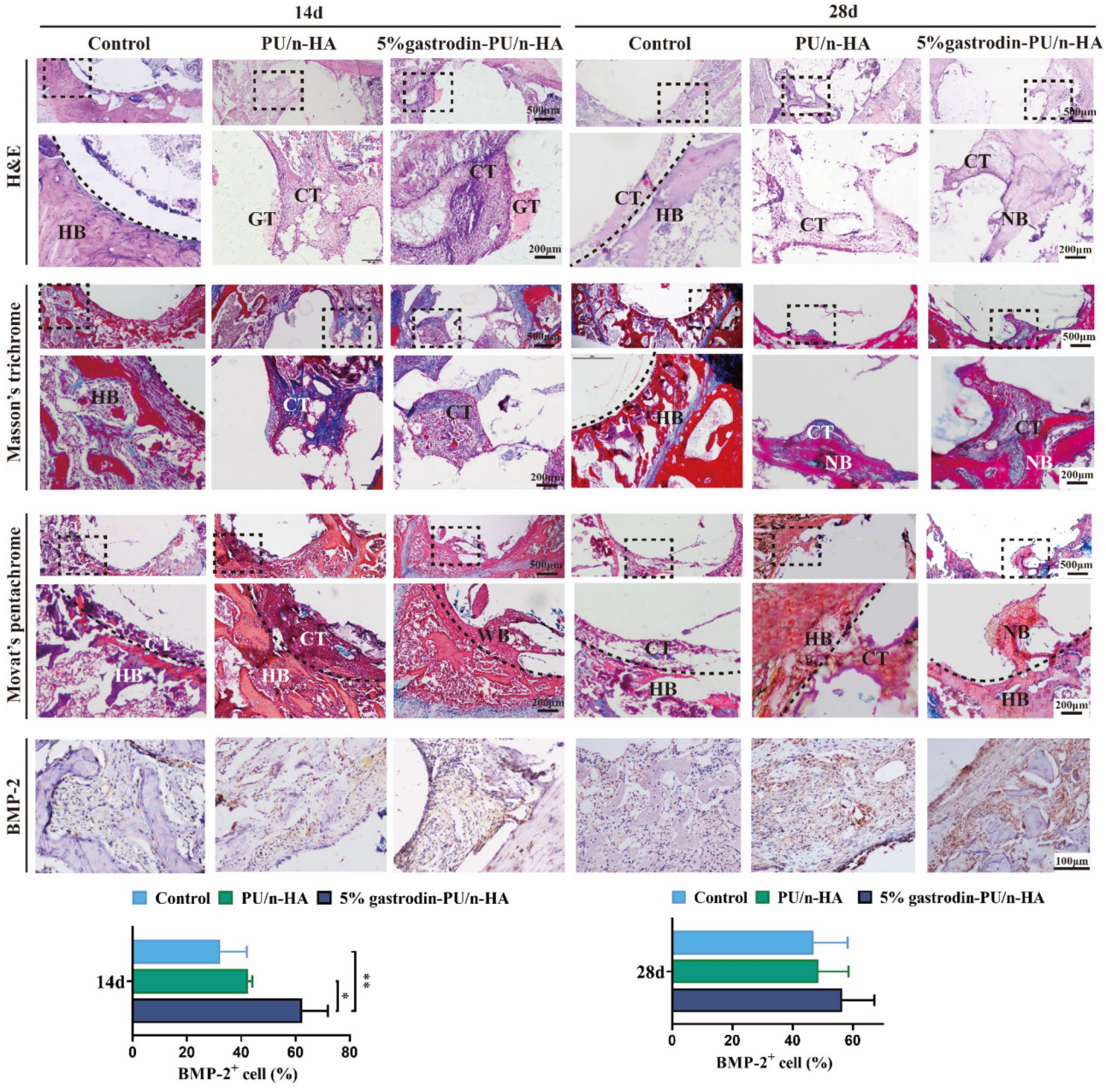

Fig. 8 Histological analysis of regenerating new bone assessed by H&E staining, Masson's trichrome staining, Movat's pentachrome staining (red-bone; blue-cartilage; dark red-connective tissue), and IHC staining for the osteogenic marker BMP-2 and its semiquantification of positively stained cells. (HB: host bone; WB: woven bone; NB: new bone; CT: connective tissue; GT: granulation tissue) Error bars represent standard deviation from mean ($n=3$). $^{**}p<0.01$; $^{*}p<0.05$

large amount of ingrown granulation tissue and connective tissue within the defect area in the implanted groups at both 14 and 28 days. A distinctive feature was the largest area of newly bone matrix indicative of osteogenic activity in the 5% gastrodin-PU/n-HA after 28 days compared with other groups. Scaffolds-mediated bone regeneration was confirmed by Masson's trichrome staining. The repairation of implanted groups had significant advantage compared with controls at both endpoints. Moreover, connective/stromal-like tissues extended along the periphery of host bone and infiltrated inside the pores of scaffold. This had apparently contributed partly to the formation of neo-bone in the 5% gastrodin-PU/n-HA. Movat's pentachrome staining allowed further identification of tissue components with high-mineralized tissue in red and low-mineralized tissue in dark red at the regeneration site. As expected, the 5% gastrodin-PU/n-HA group exhibited more prominent deposition of

woven bone. Although only loose connective tissues were observed in the PU/n-HA group, it appeared to be superior to control group in terms of new tissue formation.

Consistent with the histological staining results, BMP-2 staining validated the possible osteogenic-related expression. A large number of BMP-2 (an inducer of osteogenic differentiation) positive cells (in brown) were observed at 14 days in 5% gastrodin-PU/n-HA group, which was significantly higher than that in the PU/n-HA group; only occasional BMP-2 positive cells were observed in the control group. The continued differential expression of osteogenic marker BMP-2 and formation of neo-bone tissue were time-dependently increased at different time points in all groups. Very strikingly, in the 5% gastrodin-PU/n-HA group, BMP-2 positive expression was progressively augmented to the extent that exceeded our previous findings with respect to repair efficiency of gastrodin releasing scaffold.

In Micro-CT reconstruction, neo-bone formation within the defect area was our region of interest at 28 days post-implantation. Compared with control, the implanted groups exhibited more new bone within the defect region, wherein 5% gastrodin-PU/n-HA achieved the most apparent bone repair (Fig. 9A). Based on a large number of 2D sections, we drew a conclusion that 5% gastrodin-PU/n-HA was an osteogenic enhancer (Fig. 9B). Neo-bone tissue extended around the 5% gastrodin-PU/n-HA scaffolds and infiltrated into the pores. The PU/n-HA group presented a less osteogenic tendency to enwrap the remaining materials; moreover, new bone ingrowth to bridge two distant walls was diminished. In the control group, neo-bone was mainly confined to the margins of the outermost defect. Quantitative data showed that the BV/TV and Tb.N in the 5% gastrodin-PU/n-HA group were significantly higher than those in PU/n-HA and control groups (Fig. 9C). Regarding degenerative changes in osteoporosis, we next focused on performing an in-depth microstructural analysis. As shown in Fig. 9D, the 5% gastrodin-PU/n-HA group exerted obvious protective effects on the host trabecular bone adjacent to the implants, presenting a uniform trabecular bone distribution. Finite element analysis (FEA) confirmed a more homogenous distribution of deformation in 5% gastrodin-PU/n-HA upon loading, while an obvious concentration of maximum deformation was visualized in control group. Further analysis demonstrated that the PU/n-HA group had generally higher BV/TV, Tb.Th, Tb.N, BMD than the control group (Fig. 9E). This was especially evident in 5% gastrodin-PU/n-HA group in which a prominently higher Tb.N and lower Tb.sp were observed, suggesting efficient alleviation in development of osteoporosis. Taken together, the present results have shown unequivocally that 5% gastrodin-PU/n-HA can contribute to endogenous bone regeneration within defect regions and more importantly, it reverses the bone loss due to progression of osteoporosis.

Discussion

Osteoporosis has an insufficient bone regenerative capacity, and once a bone defect occurs, an inflammatory response always appears, leading to damaged stem cell function and delayed healing. There are two essential steps to synergistically regulate bone repair: early-staged recruitment of stem cells to lesion sites, followed by their differentiation into osteoblasts and mineralization of extracellular matrix. For this reason, developing regeneration-driven biomaterials to mimic physiology staged microenvironment was proposed for the fabrication of PU/n-HA scaffolds with sequential gastrodin-release system. Our group had previously established a PU/n-HA platform to locally control gastrodin release and this had yielded reasonable bone regenerate effect in an experimentally created condylar defect of femur model in SD rat. When subcutaneously implanted, the scaffold attenuated fibrous capsule formation. No pathological changes in the major organ tissue (heart, liver, spleen, kidney, and lung) were found in histological specimens [18]. The low porosity and slow degradation, however, had limited the infiltration of regenerating tissues into center of the bio-scaffold. Here, we modified the foaming method by enlarging the pore size and porosity *via* adjusting the composition proportion and foaming agent, to obtain a uniform porous scaffold (Fig. 1C). The microporous structure was comparable to the cancellous bone that can accommodate cell niches for osteoporotic bone regeneration. During in vitro degradation, the newly fabricated scaffolds were demonstrated to release gastrodin in a gradient concentration (Fig. 1A and B), which would satisfy the greater gastrodin demands for remodeling microenvironment and guide the sequential behaviors of endogenous stem cells.

Enhancing the homing of endogenous stem cells contributes to in situ tissue repair. The acute inflammation upon implantation can activate local and circulating monocytes/macrophages to defect region and release excess chemokines, cytokines, and other factors [29, 30]. Chemokines, as representative sensors of inflammatory microenvironment, have capability to trigger the migration and enrichment of host mesenchymal stem cells (MSCs) and osteoprogenitor cells from their local niches [31]. The major chemokine involved in this is related to SDF-1α/CXCR4 signal axis [32]. Bone marrow (BM) is considered the main reservoir of many stem cells. It is well documented that BM-derived stem cells (BMSCs) increase the quantity of available regenerative cells for the repair of remotely injured tissue through mobilization or homing [33]. The present results have shown that microenvironmentally optimized scaffold produced

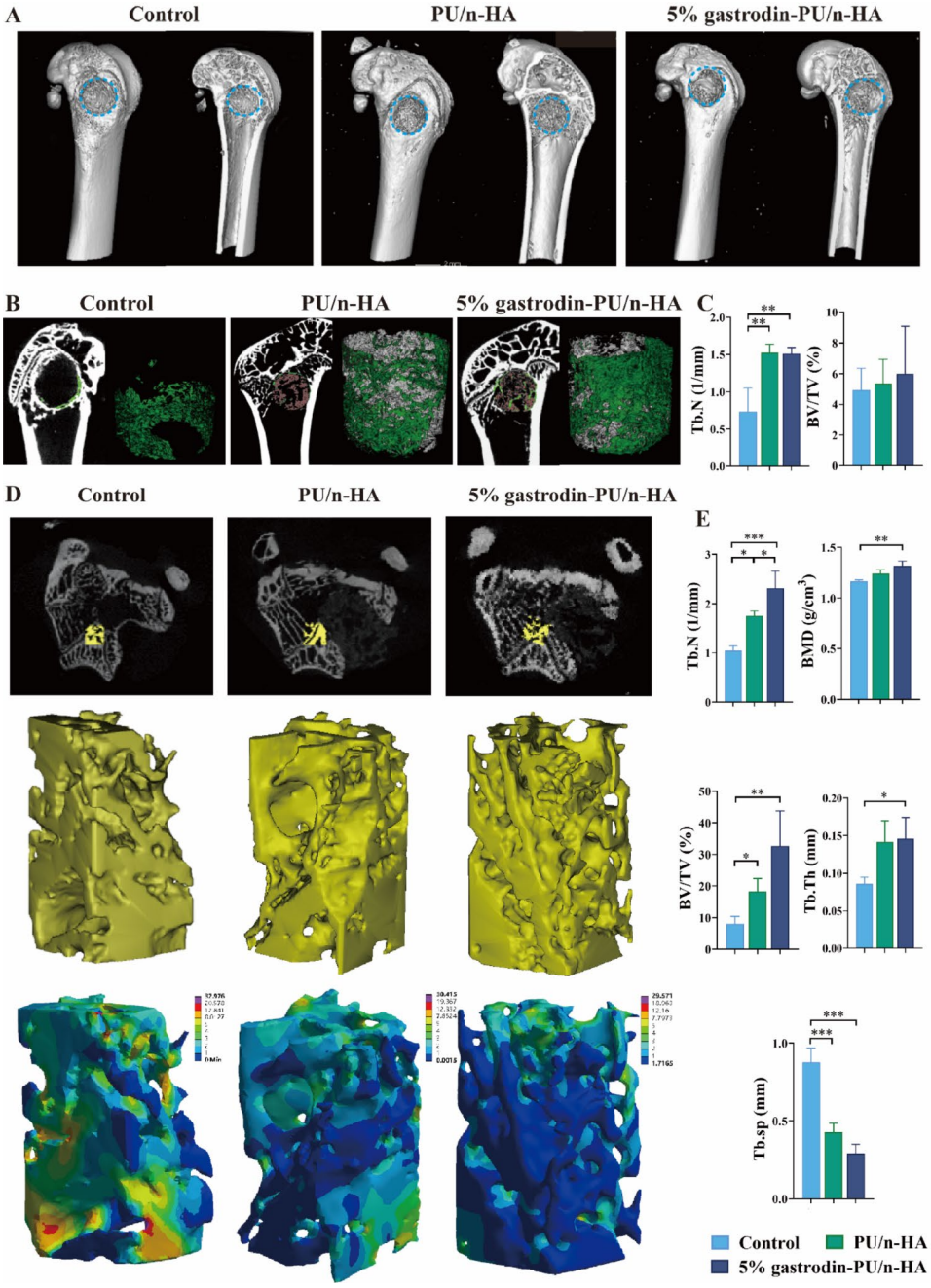

Fig. 9 In vivo bone healing evaluation on an osteoporotic rat model with bone defect. (**A**) Representative reconstructed 3D micro-CT images of bone tissue. (**B**) 2D cross-sectional images (left panel) and 3D micro-CT rendered images (right panel) of the implant-new bone within defective area. (**C**) Quantitative analysis of the parameters (Tb.N and BV/TV) of regenerative bone ($n=3$). (**D**) First panel: 2D cross-sectional images of femoral condyles; second panel: 3D micro-CT rendered images of the trabecular bone adjacent to the defect; third panel: FEA predicted total deformation under load. (**E**) Quantitative estimation of BV/TV, Tb.Th, Tb.sp, Tb.N, BMD. Error bars represent standard deviation from mean ($n=3$). ***$p<0.001$; **$p<0.01$; *$p<0.05$

sufficient cell migration-related genes (SDF-1 and TGF-β) (Fig. 3D and F) to recruit more cell to lesion in vivo. This is evidenced by activation of BMSCs population within the bone marrow. Thus, the number of $CD29^{+}$/$CD45^{-}$/$CD90^{+}$ in the 5% gastrodin-PU/n-HA group was substantially higher than those in both PU/n-HA and control groups (Fig. 3B). This notion lends its support from the transwell system as designed by us. In this connection, an inductive microenvironment created by scaffolds retrieved from subcutaneous or femoral condyle defect, to direct BMSCs migration in transwell system was also designed, and 5% gastrodin-PU/n-HA preferentially upregulated their migration rate (Fig. 3C and E).

In addition to inducing stem cells to reach the bone defect area, endogenous bone regeneration requires that not only renewal of the stem cell population but it also needs to ensure osteogenic differentiation. In the latter, appropriate and timely switch toward M2 type macrophage has been widely recognized as necessary in the process of endogenous stem cell recruitment and behavior [34]. In agreement with other osteoinductive biomaterials, our scaffold promoted polarization of M2 macrophages phenotype which provided pro-healing factors (Fig. 2D and E). This had extended a cytoprotective effect and promoted cell survival at the defect site. Additionally, serum biomarker analysis showed a lower level of proinflammatory cytokines in the 5% gastrodin-PU/n-HA group than in the PU/n-HA group (Fig. 2A-C). Furthermore, stimulated stem cells underwent proliferation following injury [35]. Here we showed an increase in population of EdU-labeled proliferating BMSC when treated with 5% gastrodin-PU/n-HA implant, indicating its potential in enhancing regeneration through proliferation (Fig. 4A and B).

Mitochondria, the essential organelles that are responsible for energy production and cellular processes (e.g., cell growth/differentiation), had capability to proliferate while maintaining cell viability [36, 37]. Improvement in mitochondrial function-related genes and proteins (PGC1α, ATP5A1, Mtco2, and TOM20), mitochondrial area, and mitochondrial membrane potential expression (Fig. 4) induced by 5% gastrodin-PU/n-HA treatment at all time points showed its potential to rescue the mitochondrial damage associated with inflammation. A large F-actin assembly and spreading area of BMSCs treated with 5% gastrodin-PU/n-HA were significantly enhanced, reflecting activated BMSCs. Upon initiation of osteo-differentiation process, the perinuclear mitochondria became more uniformly distributed throughout the cytoplasm, which may fulfill a greater energy demand. Interestingly, the stem cell and osteogenic differentiation markers (OCT-4 and OSX), were enriched asymmetrically in the dividing cell pairs (Fig. 5A). After osteogenic induction, the activation of osteogenic transcription factors, including Runx2, OSX, and BMP-2, was enhanced in 5% gastrodin-PU/n-HA group (Fig. S1), indicating osteo-differentiation is initiated in this condition to adapt to the growth microenvironment.

The balance between stemness and osteo-differentiation probably hinges on the precise regulation in asymmetric cell division. Once the stem cells leave their niche, they proliferate and divide asymmetrically to maintain a balance of dividing and differentiating cells within a tissue, generating one progenitor and one differentiated cell toward desired phenotype [38, 39]. The process of ACD relies on the differential portioning of niche contacts [40] and evolutionarily conserved polarity complex Par-3(Baz)/Par-6/aPKC [21]. The fate determining par complex is asymmetrically segregated, leading to opposing fate of two daughter cells, as well as distinct polarity-driven functions [41]. With respect to polarization of fate determinant, aPKC protein was asymmetrically distributed in some dividing cell pairs when treated with 5% gastrodin-PU/n-HA implant (Fig. 6A-C). Elevated aPKC gene expression was shown to trigger ACD (Fig. 6D). On the other side, polarized Wnt signaling was probably responsible for asymmetric cell division, which regulates tissue polarity and cell patterning. Experiments confirmed that overexpression of Wnt ligands in hematopoietic stem cells [42] or active β-catenin in conjunctival stem cells [43] results in an increased number of stem cells. The pivotal role of Wnt-β-catenin signaling in bone homeostasis is exemplified by its strong link with PTH and BMP [44]. Okuchi et al. recently demonstrated that immobilized-Wnt materials can accelerate bone repair by maintaining stem and osteogenic cells in the injury site [26]. In the present study, the 5% gastrodin-PU/n-HA implant strongly upregulated osteogenesis related genes and pathways related to ACD, including the Wnt, aPKC signaling pathway. The colocalization of β-catenin with OCT-4 in one daughter stem cell indicated the involvement of Wnt in the course of ACD (Fig. S5). In other words, their synergistic functions had facilitated asymmetric outcome of the division. Furthermore, some stem cells undergo proliferating symmetric division to give rise to two daughter stem cells are also needed [45]. Such symmetric division would critically expand stem cell population, especially when neo-tissues increase in size after injury [20]. We showed here that as tissue regenerated, stem cell associated marker OCT4 was expressed at high levels in the 5% gastrodin-PU/n-HA group (Fig. 5A, B and D), indicating expansion of stem cell population, necessary for new tissue formation.

Effective matrix cell-trapping within the bone defected or scaffold site is a guarantee for bone repair. Skeletal stem/progenitor cells (SSCs) have been recently characterized as tissue-specific stem cells in skeletons and are in favor for bone development and regeneration [46–48]. SSCs have been shown to give rise to osteoblasts, making it necessary to determine their fate selection. In the present results, the SSCs also appear to be dedicated to ensuring asymmetric outcome of the division, therefore one that supports self-renewal and another that promotes differentiation (Fig. 7). It is tempting to speculate that the stem cells consisting of the resident cells in the matrix and marrow both can contribute significantly to the maintenance of homeostasis. Thus, confirming the satisfactory efficiency of 5% gastrodin-PU/n-HA scaffold in osteoporotic bone regeneration in vivo is crucial. In our osteoporotic rat femur defect model, the 5% gastrodin-PU/n-HA implant induced higher positive-BMP-2

expression in new bone tissues (Fig. 8). Interestingly, this is coincident with the attenuated inflammatory microenvironment now exposed to reparative factors regulated by M2 macrophages (Fig. 2D and E). After implantation for 14 days, the early tissue repaired with the 5% gastrodin-PU/n-HA presented more connective tissue infiltration and regeneration. It is well documented that MSCs are progenitors of connective tissues. The 5% gastrodin-PU/n-HA scaffold had exerted a significant regulatory effect on MSCs, mainly enriching CD146 (Fig. 3A) and BMP-2 markers to maintain the stem cell pool and osteogenic differentiation. This apparent regenerative advantage was even more pronounced at 28 days after implantation. While maintaining the number of stem cells, the 5% gastrodin-PU/n-HA group had exhibited largest bone area and osteoblast numbers. Ameliorating bone loss near the implant is interesting because continuing osteoporosis could cause undesirable microenvironment known to insufficient bone repair [49, 50]. Our micro-CT analysis revealed that the implanted groups had more promising outcome in maintaining the adjacent osteoporotic trabecular microstructural parameters (Fig. 9). The advantageous repair effect of 5% gastrodin-PU/n-HA scaffold may benefit from a conducive environment with continuous gastrodin release. In synergy with the early mechanical support rendered by scaffold, which could share load distribution with the adjacent osteoporotic bone, osteoporosis had significantly improved. Taken together, we have showed that the osteoporotic bone regeneration by 5% gastrodin-PU/n-HA group was superior to that of PU/n-HA and control groups, suggesting that an optimized microenvironment might sufficiently regulate cell fate in the repair process and eventually regenerate bone tissues.

As far as we know, there is little experimental evidence supporting the distinct fate of stem cells after implantation of scaffolds during the regeneration of defective bone. Our present repair strategy merely aims to explore the potential in self-renewal and osteo-differentiation of stem cells isolated from both bone marrow and skeleton, which is a relatively confined approach. The main limitations of the study include the lack of a purification process for stem cells, which might further help identify the precise fate of stem cells. Further decode of exact ACD manner, including osteogenic commitment of recruited stem cells mediated by gastrodin-optimized microenvironment, may improve the bone repair strategy to even a higher level.

Conclusion

The mechanism of microenvironmentally optimized gastrodin-functionalized PU/n-HA in orchestrating osteogenic commitment of recruited stem cells was elucidated in the present study. The gastrodin-PU/n-HA scaffold had a dual role in endogenous bone regeneration by promoting recruitment of stem cells and induction of osteogenic differentiation. When the scaffold implantation, endogenous stem cells or progenitors were activated and migrated to the lesion, which subsequently strongly enhances stem cell population and osteogenic niches by facilitating M2 macrophage polarization. We further revealed that both recruited BMSC and SSC-like cells utilized asymmetric cell division to balance stemness maintenance and differentiation, which were governed by distinct aPKC and β-catenin biases. These findings could give important inspiration for mimicking the endogenous bone regeneration in a stem cell fate perspective.

Supplementary Information

The online version contains supplementary material available at https://doi.org/10.1186/s12951-024-02886-7.

Supplementary Material 1

Supplementary Material 2

Author contributions

S.P. and Y.L. designed the study; S.P., L.W., Y.G., K.X., G.F., Y.H., X.L., and S.Q. performed the research. S.P., Y.L., and Q.L. analyzed the data. S.P. wrote the manuscript. L.G. and L.L. edited the manuscript. L.G. and L.L. provided insights of the study and supervised the project.

Funding

This project was funded by National Natural Science Foundation of China (grant no. 82260366, 82160175), Yunnan Science and Technology Program (202201AT070136, 202301AY070001-032, 202001AY070001-014, 2018FE001(-125)), Bai Xiaochun expert workstation (YSZJGZZ-2020040).

Data availability

No datasets were generated or analysed during the current study.

Declarations

Competing interests

The authors declare no competing interests.

Author details

[1]Yunnan Key Laboratory of Stem Cell and Regenerative Medicine, School of Rehabilitation, Kunming Medical University, Kunming 650500, China
[2]Department of Stomatology, The First People's Hospital of Yunnan Province, Kunming 650032, China
[3]Department of Neurology, The First Affiliated Hospital, Kunming Medical University, Kunming 650032, China
[4]Department of Endocrinology, The Third People's Hospital of Yunnan Province, Kunming 650011, China

Received: 12 July 2024 / Accepted: 30 September 2024
Published online: 20 November 2024

References

1. Xu Y, Chen C, Hellwarth PB, Bao X. Biomaterials for stem cell engineering and biomanufacturing. Bioact Mater. 2019;4:366–79.
2. Mitrousis N, Fokina A, Shoichet MS. Biomaterials for cell transplantation. Nat Reviews Mater. 2018;3:441–56.
3. Gaharwar AK, Singh I, Khademhosseini A. Engineered biomaterials for in situ tissue regeneration. Nat Reviews Mater. 2020;5:686–705.

4. Fu X, Liu G, Halim A, Ju Y, Luo Q. Song, Guanbin: Mesenchymal Stem Cell Migration and tissue repair. Cells; 2019. p. 8.
5. Safina I, Embree MC. Biomaterials for recruiting and activating endogenous stem cells in situ tissue regeneration. Acta Biomater. 2022;143:26–38.
6. Xia H, Li X, Gao W, Fu X, Fang RH, Zhang L, Zhang K. Tissue repair and regeneration with endogenous stem cells. Nat Reviews Mater. 2018;3:174–93.
7. Zhang H, Yu S, Zhao X, Mao Z, Gao C. Stromal cell-derived factor-1α-encapsulated albumin/heparin nanoparticles for induced stem cell migration and intervertebral disc regeneration in vivo. Acta Biomater. 2018;72:217–27.
8. Zhang X, Jiang W, Xie C, Wu X, Ren Q, Wang F, Shen X, Hong Y, Wu H, Liao Y, et al. Msx1(+) stem cells recruited by bioactive tissue engineering graft for bone regeneration. Nat Commun. 2022;13:5211.
9. Pajarinen J, Lin T, Gibon E, Kohno Y, Maruyama M, Nathan K, Lu L, Yao Z, Goodman SB. Mesenchymal stem cell-macrophage crosstalk and bone healing. Biomaterials. 2019;196:80–9.
10. Li X, Li C, Zhang W, Wang Y, Qian P, Huang H. Inflammation and aging: signaling pathways and intervention therapies. Signal Transduct Target Ther. 2023;8:239.
11. Sadowska JM, Wei F, Guo J, Guillem-Marti J, Lin Z, Ginebra MP, Xiao Y. The effect of biomimetic calcium deficient hydroxyapatite and sintered beta-tricalcium phosphate on osteoimmune reaction and osteogenesis. Acta Biomater. 2019;96:605–18.
12. Peng Z, Wang S, Chen G, Cai M, Liu R, Deng J, Liu J, Zhang T, Tan Q, Hai C. Gastrodin alleviates cerebral ischemic damage in mice by improving antioxidant and anti-inflammation activities and inhibiting apoptosis pathway. Neurochem Res. 2015;40:661–73.
13. Xiao MM, Zhang YQ, Wang WT, Han WJ, Lin Z, Xie RG, Cao Z, Lu N, Hu SJ, Wu SX, et al. Gastrodin protects against chronic inflammatory pain by inhibiting spinal synaptic potentiation. Sci Rep. 2016;6:37251.
14. Xiao G, Tang R, Yang N, Chen Y. Review on pharmacological effects of gastrodin. Arch Pharm Res. 2023;46:744–70.
15. Dai JN, Zong Y, Zhong LM, Li YM, Zhang W, Bian LG, Ai QL, Liu YD, Sun J, Lu D. Gastrodin inhibits expression of inducible NO synthase, cyclooxygenase-2 and proinflammatory cytokines in cultured LPS-stimulated microglia via MAPK pathways. PLoS ONE. 2011;6:e21891.
16. Yao YY, Li R, Guo YJ, Zhao Y, Guo JZ, Ai QL, Zhong LM, Lu D. Gastrodin attenuates Lipopolysaccharide-Induced Inflammatory Response and Migration via the Notch-1 signaling pathway in activated Microglia. Neuromolecular Med. 2022;24:139–54.
17. Yao YY, Bian LG, Yang P, Sui Y, Li R, Chen YL, Sun L, Ai QL, Zhong LM, Lu D. Gastrodin attenuates proliferation and inflammatory responses in activated microglia through Wnt/beta-catenin signaling pathway. Brain Res. 2019;1717:190–203.
18. Li L, Li Q, Gui L, Deng Y, Wang L, Jiao J, Hu Y, Lan X, Hou J, Li Y, Lu D. Sequential gastrodin release PU/n-HA composite scaffolds reprogram macrophages for improved osteogenesis and angiogenesis. Bioact Mater. 2023;19:24–37.
19. Venkei ZG, Yamashita YM. Emerging mechanisms of asymmetric stem cell division. J Cell Biol. 2018;217:3785–95.
20. Inaba M, Yamashita YM. Asymmetric stem cell division: precision for robustness. Cell Stem Cell. 2012;11:461–9.
21. Liu Z, Yang Y, Gu A, Xu J, Mao Y, Lu H, Hu W, Lei Q-Y, Li Z, Zhang M et al. Par complex cluster formation mediated by phase separation. Nat Commun. 2020;11:2266.
22. Aranda V, Nolan ME, Muthuswamy SK. Par complex in cancer: a regulator of normal cell polarity joins the dark side. Oncogene. 2008;27:6878–87.
23. Kobayashi Y, Uehara S, Udagawa N, Takahashi N. Regulation of bone metabolism by wnt signals. J Biochem. 2016;159:387–92.
24. Kramer I, Halleux C, Keller H, Pegurri M, Gooi JH, Weber PB, Feng JQ, Bonewald LF, Kneissel M. Osteocyte Wnt/beta-catenin signaling is required for normal bone homeostasis. Mol Cell Biol. 2010;30:3071–85.
25. Peng Z, Niu S, Gui L, Kuang X, Li F, Chen B, Li W, Jiao J, Lu S, Lu D. Wnt3a loaded deformable hydrogel acts as a 3D culture platform for in situ recruitment of stem cells to efficiently repair bone defects via the asymmetric division. Chem Eng J. 2022;442:136163.
26. Okuchi Y, Reeves J, Ng SS, Doro DH, Junyent S, Liu KJ, El Haj AJ, Habib SJ. Wnt-modified materials mediate asymmetric stem cell division to direct human osteogenic tissue formation for bone repair. Nat Mater. 2021;20:108–18.
27. Li Y, Yue J, Liu Y, Wu J, Guan M, Chen D, Pan H, Zhao X, Lu WW. Strontium regulates stem cell fate during osteogenic differentiation through asymmetric cell division. Acta Biomater. 2021;119:432–43.
28. PD S. Changes in skeletal mass and fragility with castration in the rat; a model of osteoporosis. J Am Geriatr Soc. 1969;17:2.
29. Shi C, Pamer EG. Monocyte recruitment during infection and inflammation. Nat Rev Immunol. 2011;11:762–74.
30. Chen S, Saeed A, Liu Q, Jiang Q, Xu H, Xiao GG, Rao L, Duo Y. Macrophages in immunoregulation and therapeutics. Signal Transduct Target Ther. 2023;8:207.
31. Cuesta-Gomez N, Graham GJ, Campbell JDM. Chemokines and their receptors: predictors of the therapeutic potential of mesenchymal stromal cells. J Transl Med. 2021;19:156.
32. Won YW, Patel AN, Bull DA. Cell surface engineering to enhance mesenchymal stem cell migration toward an SDF-1 gradient. Biomaterials. 2014;35:5627–35.
33. Chen L, Luo W, Wang Y, Song X, Li S, Wu J, Sun L. Directional homing of glycosylation-modified bone marrow mesenchymal stem cells for bone defect repair. J Nanobiotechnol. 2021;19:228.
34. Lu G, Xu Y, Liu Q, Chen M, Sun H, Wang P, Li X, Wang Y, Li X, Hui X et al. An instantly fixable and self-adaptive scaffold for skull regeneration by autologous stem cell recruitment and angiogenesis. Nat Commun. 2022;13:2499.
35. Brock CK, Wallin ST, Ruiz OE, Samms KM, Mandal A, Sumner EA, Eisenhoffer GT. Stem cell proliferation is induced by apoptotic bodies from dying cells during epithelial tissue maintenance. Nat Commun. 2019;10:1044.
36. Chen W, Zhao H, Li Y. Mitochondrial dynamics in health and disease: mechanisms and potential targets. Signal Transduct Target Ther. 2023;8:333.
37. Giacomello M, Pyakurel A, Glytsou C, Scorrano L. The cell biology of mitochondrial membrane dynamics. Nat Rev Mol Cell Biol. 2020;21:204–24.
38. Lechler T, Mapelli M. Spindle positioning and its impact on vertebrate tissue architecture and cell fate. Nat Rev Mol Cell Biol. 2021;22:691–708.
39. Morrison SJ, Kimble J. Asymmetric and symmetric stem-cell divisions in development and cancer. Nature. 2006;441:1068–74.
40. Chhabra SN, Booth BW. Asymmetric cell division of mammary stem cells. Cell Div. 2021;16:5.
41. Goulas S, Conder R, Knoblich JA. The Par complex and integrins direct asymmetric cell division in adult intestinal stem cells. Cell Stem Cell. 2012;11:529–40.
42. Goessling W, North TE, Loewer S, Lord AM, Lee S, Stoick-Cooper CL, Weidinger G, Puder M, Daley GQ, Moon RT, Zon LI. Genetic interaction of PGE2 and wnt signaling regulates developmental specification of stem cells and regeneration. Cell. 2009;136:1136–47.
43. Jang E, Jin S, Cho KJ, Kim D, Rho CR, Lyu J. Wnt/beta-catenin signaling stimulates the self-renewal of conjunctival stem cells and promotes corneal conjunctivalization. Exp Mol Med. 2022;54:1156–64.
44. Baron R, Kneissel M. WNT signaling in bone homeostasis and disease: from human mutations to treatments. Nat Med. 2013;19:179–92.
45. Gotz M, Huttner WB. The cell biology of neurogenesis. Nat Rev Mol Cell Biol. 2005;6:777–88.
46. Feng H, Jiang B, Xing W, Sun J, Greenblatt MB, Zou W. Skeletal stem cells: origins, definitions, and functions in bone development and disease. Life Med. 2022;1:276–93.
47. Li Q, Xu R, Lei K, Yuan Q. Insights into skeletal stem cells. Bone Res. 2022;10:61.
48. Chan CKF, Gulati GS, Sinha R, Tompkins JV, Lopez M, Carter AC, Ransom RC, Reinisch A, Wearda T, Murphy M, et al. Identification of the human skeletal stem cell. Cell. 2018;175:43–e5621.
49. Liu W, Wang T, Zhao X, Dan X, Lu WW, Pan H. Akermanite used as an alkaline biodegradable implants for the treatment of osteoporotic bone defect. Bioact Mater. 2016;1:151–9.
50. Luo ZH, Ma JX, Zhang W, Tian AX, Gong SW, Li Y, Lai YX, Ma XL. Alterations in the microenvironment and the effects produced of TRPV5 in osteoporosis. J Transl Med. 2023;21:327.

Publisher's note